Universidade Federal de São Carlos– UFSCar
Centro de Ciências Exatas e de Tecnologia– CCET
Departamento de Computação– DC
Programa de Pós-Graduação em Ciência da Computação– PPGCC

Rafael da Costa Silva

Partial automation of the seismic to well tie with the matching region estimation and segmented global optimization

São Carlos
2023

Rafael da Costa Silva

Partial automation of the seismic to well tie with the matching region estimation and segmented global optimization

Dissertação apresentada ao Programa de Pós-Graduação em Ciência da Computação do Centro de Ciências Exatas e de Tecnologia da Universidade Federal de São Carlos, como parte dos requisitos para a obtenção do título de Mestre em Ciência da Computação.

Área de concentração: Inteligência Artificial

Supervisor: Diego Furtado Silva

São Carlos
2023

UNIVERSIDADE FEDERAL DE SÃO CARLOS

Centro de Ciências Exatas e de Tecnologia
Programa de Pós-Graduação em Ciência da Computação

Folha de Aprovação

Defesa de Dissertação de Mestrado do candidato Rafael da Costa Silva, realizada em 13/07/2023.

Comissão Julgadora:

Prof. Dr. Diego Furtado Silva (UFSCar)

Prof. Dr. Ricardo Cerri (UFSCar)

Prof. Dr. Ricardo Araújo Rios (UFBA)

O Relatório de Defesa assinado pelos membros da Comissão Julgadora encontra-se arquivado junto ao Programa de Pós-Graduação em Ciência da Computação.

I dedicate this work to my grandparents,
who have always encouraged me to study and pursue my dreams.

Acknowledgements

Acknowledgments to Diego Furtado Silva, who guided this work, allowing me to develop the critical thinking skills of a researcher. I want to thank Marcelus Glaucus de Souza Araujo, a Geophysicist at Petrobras, for patiently explaining the fundamental concepts necessary for understanding the addressed problem and enriching our weekly meetings. With the support of both individuals, I achieved significant results in this work.

Special thanks to all those involved in the construction of the technical cooperation agreement between Petrobras and UFSCar, entitled “Algoritmo DTW para correlação de feições geológicas”, No. 13994. I am grateful for the PIDICT scholarship and recognition to CENPES and FAI.UFSCar for managing this agreement and the Exploration Executive Management of Petrobras for providing this technical challenge.

"Somos essencialmente profissionais do sentido. Educamos, quando ensinamos com sentido. Educar é impregnar de sentido a vida. A profissão docente está centrada na vida, no bem querer."
(Prof. Gilberto Teixeira)

Resumo

A interpretação geofísica desempenha um papel fundamental no domínio da exploração de petróleo e gás. Vários métodos geofísicos podem ser empregados para extrair informações sobre a configuração geológica das rochas. A amarração poço-sísmica, que envolve associar os perfis de um poço com o sismograma observado, sendo uma atividade crucial no processamento e interpretação das amplitudes sísmicas. Durante a fase de exploração o processo de amarração sísmica ajuda o interprete na compreensão da onda sísmica e da relação tempo-profundidade do poço com a sísmica. No entanto, o ruído nos dados e as incertezas inerentes do processo tornam a amarração sísmica uma atividade demorada. Nesse contexto, propomos uma automatização significativa do processo de amarração sísmica que estima a provável região de alinhamento e alinha automaticamente os traços sísmicos por meio de uma otimização global segmentada. A região de alinhamento é estimada com base no perfil de velocidade e no alinhamento usando o algoritmo *Dynamic Time Warping* (DTW). Na maioria dos poços testados os três métodos propostos estimaram com precisão a posição da base do poço no traço sísmico. A segmentação do processo de amarração poço-sísmica é feita através do relacionamento tempo-profundidade derivado do alinhamento inicial entre o traço sintético com o sismograma observado por meio do *Constrained* DTW. A segmentação do processo de amarração com *Differential Evolution* (DE) aumentou a correlação final em todos os poços testados, com quatro deles alcançando uma correlação superior a 70%, sem causar variações de velocidade irreais.

Palavras-chave: Amarração sísmica, Automação, Segmentação poço-sísmica, DTW, Otimização global, Região de amarração.

Abstract

Geophysical interpretation plays a fundamental role in the oil and gas exploration domain. Various geophysical methods can be employed to extract information about the geological configuration of rocks. The well-to-seismic tie, which involves matching well log profiles with observed seismograms, is a crucial activity in the processing and interpreting of seismic amplitudes. During the exploration phase, the seismic tie process helps the interpreter to understand the well region's seismic wavelet and the time-depth relationship. However, data noise and inherent uncertainties make the seismic tie time-consuming. This way, we propose a significant automation of the seismic tie process that estimates the probable alignment region and automatically aligns the seismic traces through segmented global optimization. The alignment region is estimated based on the velocity profile and alignment using the DTW algorithm. The three proposed methods accurately estimated the well base position in the seismic trace for most of the tested wells. Our approach performs the segmentation of the tying process by utilizing the time-depth relationship obtained from the initial alignment of synthetic and seismic traces using *Constrained* DTW. The segmentation of the DE tying process increased the final correlation in all tested wells, with four achieving a correlation higher than 70% without causing unrealistic velocity variations.

Keywords: Well-tie, Automation, Well-seismic segmentation, DTW, Global Optimization, Matching region.

List of Figures

List of Tables

List of acronyms

BDW *Blocked Dynamic Warping*

BO Bayesian Optimization

CNN Convolution Neural Networks

DTW *Dynamic Time Warping*

DE *Differential Evolution*

DE-tie Differential Evolution for Well Tie

ED Euclidean distance

GAP Global Average Pooling

GP Gaussian process

MD Measured Depth

PSO Particle Swarm Optimization

QC Quality Control

TVDSS True Vertical Depth Sub Sea

TVD True Vertical Depth

TWDTW Time-weighted Dynamic Time Warping

VSP Vertical Seismic Profile

List of algorithms

Contents

Chapter 1

Introduction

In petroleum and gas exploration, geophysics interpretation develops a fundamental role. The decision to drill for petroleum or minerals in a determined location often depends on the interpreter's capacity to build the study region's earth model using the available data. Usually, the modeling process needs to integrate data from geology, geophysics, and the case of petroleum exploration, petrophysics, and reservoir engineering (LINES; NEWRICK, 2004; SIMM; BACON, 2014). Despite the wide range of interpretation lenses like seismic, gravity, and magnetic, this work is inserted in the context of seismic amplitude interpretation principally to find and exploit hydrocarbons (fossil fuels). Seismic amplitude interpretation is fundamental to technical evaluation and decision-making at all upstream oil and gas business stages. This kind of interpretation allows us to estimate the changes in geologic formations and interpolate the information between two wells[1]. Correlating the seismic data with the well data is essential during interpretation. This seismic-to-well tie activity aims to align a seismic trace with a synthetic trace derived from the well data.

We obtained the seismic trace from an acquisition survey. Its concept is simple: the energy source in marine acquisition airguns produces seismic waves that travel through the subsurface. Each receiver on the cable records the energy refracted or reflected from the contrast in acoustic hardness (the impedance) associated with geological interfaces, describing the path of the sound energy by *rays* drawn perpendicular to the seismic *wavefront*. Whether the survey is on the land or sea, the data needed for seismic amplitude analysis require several traces for each surface point to effectively provide measurement

[1] Well is a drill hole designed to explore and extract production of hydrocarbons (oil and gas), it can be drilled on land (onshore well) or the sea's surface (offshore well). Font: <https://www.collinsdictionary.com/>, access on 30th match 2023.

across a range of *angles of incidence*. The marine environment provides a good setting for acquiring such data, as shown in Figure 1 (GADALLAH; FISHER, 2008; SIMM; BACON, 2014).

Figure 1 – Source and receiver configuration showing wavefronts, rays (perpendicular to wavefronts), and angle of incidence θ increasing with offset.

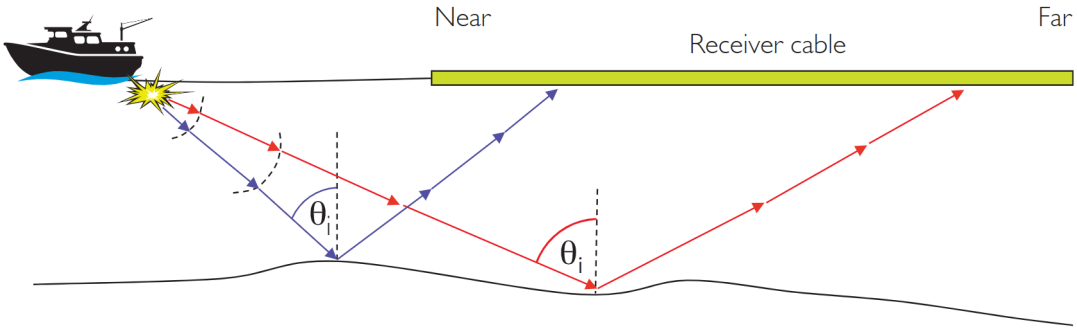

Font: Simm e Bacon (2014)

The construction of the synthetic trace requires a seismic model. The aspect of the seismic model is that we can observe the seismic trace as the convolution of a seismic pulse with a reflection coefficient related to contrasting rock properties across rock boundaries. Where the seismic pulse emulates the source wave propagated during the acquisition. Figure 2 shows a schematic illustration of the convolutional model, detailed in section 2.4. Aligning both traces is a complex activity once this model simplifies the complex seismic energy propagation with numerous factors related to geology and acquisition (SIMM; BACON, 2014). This way, even though in theory both traces represent the same event, the well-tie does not aim for a perfect match between the wave shape of both signals but an alignment good enough to identify reflectors present in the observed seismogram and in the well data (NEWRICK, 2012).

The procedure for tying a synthetic seismogram to seismic data comprehends the following steps: calibrate the well data, construct the synthetic seismogram, and perform the match by determining the best match location and aligning both traces (SIMM; BACON, 2014). In the literature, the works focused on the tying and wavelet estimation steps while finding the best match location still need to be addressed. The matching step can be considered a time series alignment activity in the computational context. Allowing general propose time series alignment algorithms like *Dynamic Time Warping* (DTW) (SAKOE; CHIBA, 1978) to create an automatic well-to-seismic algorithm. Although DTW can get a high correlation coefficient when aligning the synthetic and observed seismogram, the warping caused in the process is propagated to the Well logs, generating unrealistic variations once the original logs (Sonic and Density) have physical constraints (HERRERA; BAAN, 2014). For instance, after tying the well with the seismogram, it is

Figure 2 – Schematic illustration of the convolutional model

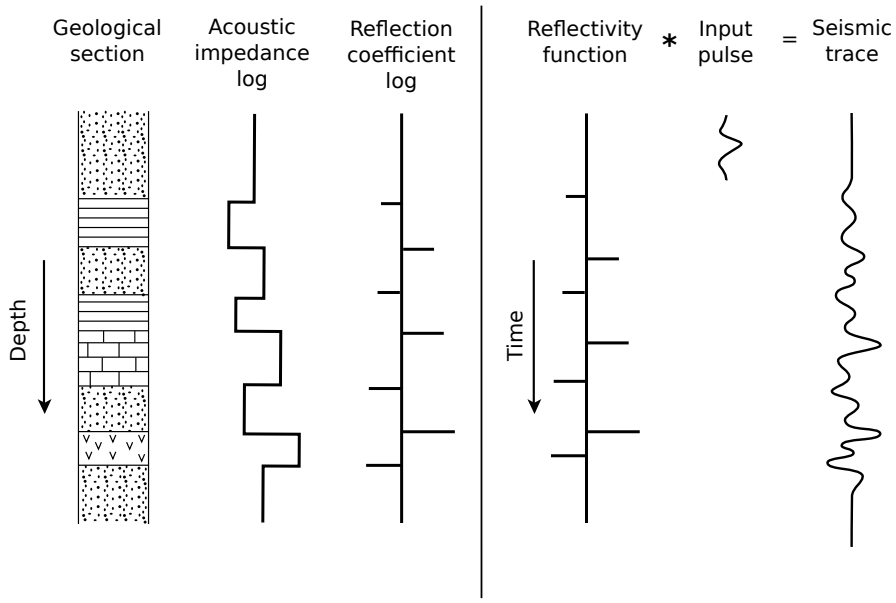

Source: Adapted from Nwafor e Hermana (2022).

physically non-realistic to have the Sonic log with a variation higher than 20% if compared with its original version (before the tying process).

The most common way to reduce the warping effect in the original logs is to apply a sakoe-chiba constraint window, defining how much warp DTW is allowed (HERRERA; BAAN, 2014). Wang, Lomask e Segovia (2017) present a more sophisticated way to mitigate the occurrence of non-realistic velocities, the *Blocked Dynamic Warping* (BDW). The BDW executes the warp at the time-shift domain (instead of the sample domain), and blocks of velocity variation models restrict the amount of allowed time-shift, similar to a sakoe-chiba window. However, this approach needs specialized knowledge or geological markers to define the block models and boundaries (each block has its own model), limiting the use of BDW in an automatic well-to-seismic tie workflow.

The use of neural networks and evolutionary algorithms has also been proposed. Wu et al. (2022) describe a method to use Convolution Neural Networks (CNN) to learn the characteristic of different waveforms. Through an *encode-decode* architecture, the neural network can encode the synthetic seismogram and decode a warped version that matches the original seismogram. However, the neural network needs to be trained specifically for the well and also has the limitation of needing geological markers to segment the synthetic log. On the other hand, Gelpi, Pérez e Velis (2020) take advantage of the link between synthetic log and well's logs and uses a global optimization algorithm, the *Differential Evolution* (DE), to perturb the velocity logs in a way to create a synthetic seismogram aligned with the observed seismogram. The great advantage of this method is that it does

not require human intervention to verify the velocity distortion, select the velocity model, or use geological markers, and it allows high control of the velocity log.

1.1 Main Contribution

The general objective of this work is to develop an automatic workflow for the well-to-seismic tie activity that can obtain an acceptable correlation coefficient higher than 70% without generating non-realistic variation in the velocity log, lower than 20%, and the user can adjust and interpret the results at any point of the execution.

Previous works focused more on the tying and wavelet estimation steps. In contrast, this work focuses on the tying and the estimation of the best match location, working specifically with offshore well data, assuming that the wavelet is known. This work concentrates on estimating the best match position and improving the performance of a well-seismic alignment method. The main contributions of this research can be summarized as follows:

- ❏ We developed an algorithm to estimate the correct match position to align the synthetic seismogram with the seismic data;
- ❏ We incorporated an optimization step to estimate the pre-processing hyper-parameters for cases where these values are unknown;
- ❏ We developed an algorithm to segment the well based on the observed seismogram through an initial alignment with DTW;
- ❏ Embedding the Well-seismic segmentation algorithm, we could improve the efficiency of the Differential Evolution for Well Tie (DE-tie) method by allowing the use of more knots and different phase rotations for each Well segment;

1.2 Dissertation Organization

This work is organized as follows:

- ❏ Chapter 2 presents the computational and domain application theoretical background necessary to understand this work. Firstly, we introduce the basic concept of time series, followed by global optimization. Finally, a brief description of seismic events, reservoir geophysics, and a detailed discussion about the well-to-seismic tie constraints comprehend the specific domain theoretical background.
- ❏ Chapter 3 provides a detailed account of the principal methods for automatic or semi-automatic alignment of seismic traces used in the well-seismic tie. After, is

presented a partial automation of the seismic well tie. The chapter concludes with a discussion of the main contributions and limitations of the methods presented.

- ❏ Chapter 4 describes our proposed segmented process for a well-seismic tie with the matching region estimation. Our process includes a novel algorithm to estimate the seismic traces alignment region and contributions to the well tie method developed by Gelpi, Pérez e Velis (2020). These contributions aim to enhance its performance in offshore wells with significant depths.

Chapter 2

Theoretical Background

This chapter presents the theoretical background used in this work. We describe distance measurements for time series and time series alignment activity, essential computational tools in the well-to-seismic tie process. Once our proposed workflow uses global optimization algorithms in a few steps, we present a general view of global optimization problems and their classical optimization algorithms. After, we introduce more information about seismic events, which complements the seismic acquisition process described in the Introduction section. Then, some reservoir geophysics concepts are presented, principally related to Well logs used in the tying process. Finally, we detail all steps and constraints in the well-to-seismic tie process.

2.1 Time Series

Time series is a common kind of data present in various human activities, for example, music, the financial market, and signal processing. This drew the attention of many researchers to propose a wide range of methods to analyze this kind of data for different temporal data mining tasks. Using a formal definition, a time series S is a sequence of N ordered values such that $S = (s_1, s_2, \ldots, s_N)$ and $s_i \in \mathbb{R}^d$ for all $i \in [1, N]$. Each value s_i is an *observation* and N is the *length* of the time series. When $d = 1$, the time series is called single-dimensional. For $d > 1$, we have a multi-dimensional time series (SILVA; BATISTA; KEOGH, 2018).

Usually, time series observations are measurements of the study object collected in equidistant time intervals, a common supposition once measurement devices (normally) record values in a constant sample rate. The term *time* here refers to the measurement domain. An example of time series is the electrocardiogram (ECG) record from dataset

ECG200 (OLSZEWSKI, 2001) present at UCR time series archive (DAU et al., 2019), Figure 3.

Figure 3 – Example of time series obtained from 8 ECG records concatenated.

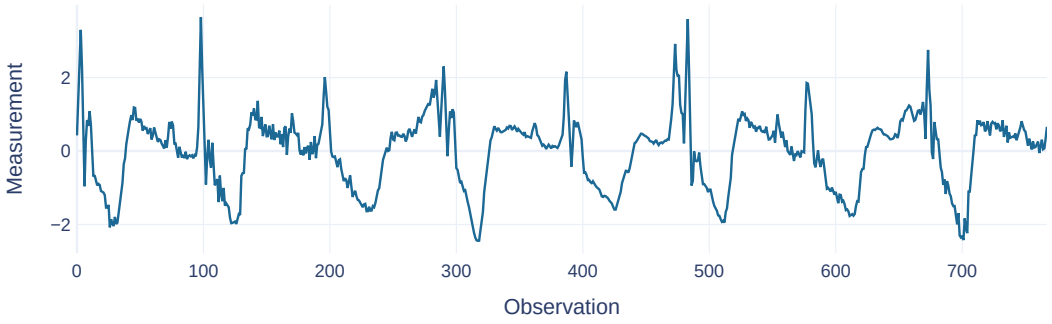

Source: Author from ECG200 (OLSZEWSKI, 2001).

2.1.1 Distance measures for time series comparing

Various time series activities need to use some distance measures for dissimilarity comparison. Those based on the Minkowski distance comprehend the most established family of distances used in dissimilarity tasks (SILVA; BATISTA; KEOGH, 2018).

$$d_{\text{minkowski}}(S, Q) = \left[\sum_{k=1}^{N}(s_k - q_k)^p\right]^{1/p} \tag{1}$$

where N is the length of both S and Q. The values s_k and q_k are the observations of those time series in the k-th position and $p \in \mathbb{N}$ is a user-defined parameter. From Equation 1, the Euclidean distance (ED) can be obtained by setting $p = 2$. Formally, we define the ED between time series S and Q as below:

$$ed(S, Q) = \sqrt{\sum_{k=1}^{N}(s_k - q_k)^2} \tag{2}$$

Any measure derived from Minkowski distance is appropriate for a time series with the same number of observations. In this way, the ED measures the dissimilarity between samples positioned at the same relative time and is not suited for comparing time series that require a nonlinear matching of observations (FOLGADO et al., 2018). In other words, assume that the features that describe the observed phenomena, like peaks and valleys, are shown at the same relative time in both time series.

The context of the well-to-seismic tie, and in many other applications, requires a more flexible matching of observations. For this, the DTW distance can achieve an

optimal nonlinear alignment of the observations under the following constraints (SILVA; BATISTA; KEOGH, 2018):

- ❏ **Boundary constraint.** The matching occurs for the whole time series S and Q, starting at $(1, 1)$ and ending at (N, M). Where $S = (s_1, s_2, \ldots, s_N)$ and $Q = (q_1, q_2, \ldots, q_M)$.
- ❏ **Monotonicity constraint.** The relative order of the observations has to be preserved.
- ❏ **Continuity constraint.** The matching is made in one-unit steps. The matching never skips one or more observations.

Figure 4 shows the difference between the linear alignment obtained from ED and the nonlinear alignment performed by DTW.

Figure 4 – The difference between the alignment obtained by ED (*left*) and DTW (*right*) between two heartbeats. Note the presence of an offset in the valley region. The alignment presented is only for visualization proposes with some processing applied before the DTW execution.

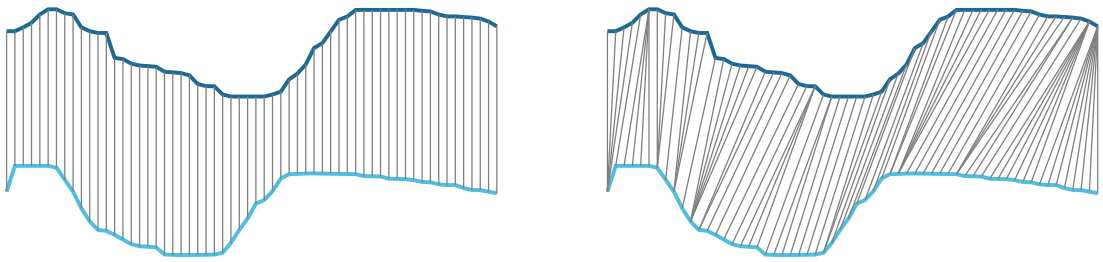

Source: Author from ECG200 (OLSZEWSKI, 2001).

A nonlinear alignment has computational complexity as a disadvantage. DTW uses a dynamic programming technique that requires processes of a quadratic cumulative cost matrix (SILVA; BATISTA; KEOGH, 2018). To work with a massive amount of data exists techniques to optimize the computational cost to compute this matrix (SILVA; BATISTA, 2016). Once the synthetic seismogram is relatively short, for this work, the DTW execution time is not a preoccupation.

2.1.2 Time series subsequence alignment

One of the DTW sub-products is the alignment produced by a nonlinear matching during the process to compute the minimal cost between time series. By relaxing the

boundary constraint, instead of matching all observations of both time series, we can align one series as a subsequence of another. This activity is called time series subsequence alignment. Align subsequence is a useful exploratory tool for time series data mining with applications in areas such as music information retrieval (ADAMS et al., 2004).

We can define this activity as given a time series $S = (s_1, s_2, ..., s_N)$ and $Q = (q_1, q_2, ..., q_M)$ of length N and M respectively, where $N < M$. The subsequence alignment aims to find the best subsequence of Q, beginning at q_i, that minimizes a similarity measurement distance to S, where i is the initial instant of the subsequence. Usually, the searched pattern is called *query*, and the time series that contains the pattern is called *target* or *reference* (FOLGADO et al., 2022).

In the context of the well-to-seismic tie, determining the best match location to align the synthetic seismogram in the observed seismogram can be seen as a subsequence alignment activity. In this case, the synthetic log is the query, the searched pattern, and the observed seismogram is the target. Of course, some constraints are necessary once the synthetic seismogram location is not arbitrary, as detailed in section 2.4.

2.2 Global Optimization

Function optimization is a task that aims to find one of its extremes, minimal or maximal. The minimization can be turned into maximization by a sign change, and vice versa. A single local minimization can solve convex functions. However, many applications face a nonconvex (or multimodal) function with multiple minima of different values. Finding just one minimum tells us a little about the globally minimal function value and strongly depends on the starting point (HARTKE, 2011). Global optimization aims to find the solution in which the objective function obtains its smallest value, the global minimum. In the absence of *a priori* information about the region A (the search region), making the measurements at several points uniformly distributed, as a grid, over the whole region seems rational. This step gives us a global picture of the function. Additional measurements can be done near prominent regions to get more accurate *local* results (TÖRN; ŽILINSKAS, 1989).

The cost of mapping is proportional to the number of measurements (evaluations of the objective function) performed. Both the cost and accuracy will be higher for finer grids. It is necessary to make *a priori* assumption to determine the mesh size of the grid. Due to the generalization of the methods, the only way to obtain information about the function is through its evaluation. The usual solution strategy consists of a global stage and a local stage. In the lack of *a priori* information, all parts of the region must be (equally) considered on the global stage. After gathering some information, some locals can be seen as more attractive than others, and more accurate solutions in these parts are wanted - this is the local stage (TÖRN; ŽILINSKAS, 1989).

2.2.1 Differential Evolution

O *Differential Evolution* (DE) is a classical, simple, and efficient algorithm for global optimization over continuous spaces proposed for Storn e Price (1997). DE is an algorithm that uses an evolutionary strategy that generates variations of parameter vectors. The algorithm aims to fulfill five requirements:

1. Ability to handle non-differentiable, nonlinear, and multimodal cost functions;
2. Parallelizability to handle computation-intensive cost functions;
3. Ease to use, with few robust (and easy to choose) control variables to guide the minimization;
4. Good convergence properties.

The algorithm is designed to be a stochastic direct search method, which fulfills the requirement (1), while an independent stochastic perturbation of the population fulfills the requirement (2). To requirement (3), the algorithm uses a self-organizing approach for the minimization method. In this strategy, the new vectors replace their predecessor if they correspond to cost function with reduced cost compared with their predecessor, allowing the search space to expand and contract without a control variable settings defined by the user. The method also has good convergence, the requirement (4).

Differential Evolution (DE) is a parallel direct search method which utilizes N D-dimensional parameters vector

$$x_{i,G}, i = 1, 2, \ldots, N \tag{3}$$

as a population for each generation G. N does not change during the minimization process. We can choose the initial vector population randomly, covering the entire parameter space, or if an initial solution $x_{\text{init},0}$ is known, the population can be generated by adding randomly distributed deviations. Through a mutation operation, DE generates new parameter vectors by adding the weighted difference between two population vectors to a target vector. For each target vector $x_{i,G}$, a mutant vector is generated according to

$$v_{i,G+1} = x_{r_1,G} + F\dot{(}x_{r_2,G} - x_{r_3,G}) \tag{4}$$

where $r_1, r_2, r_3 \in \{1, 2, \ldots, N\}$ mutually different, $N \geq 4$ (to allow this configuration) and $F > 0$. F is a real constant factor $\in [0, 2]$ which control the amplification of the $(x_{r_2,G} - x_{r_3,G})$. Figure 5 shows a two-dimensional example that illustrates this process.

The mutated parameter vectors are mixed with the parameters of another predefined vector to increase the diversity and yield the trial vector. This process is called crossover. To this, the trial vector

Figure 5 – An example of a two-dimensional cost function and the process of generating $v_{i,G+1}$.

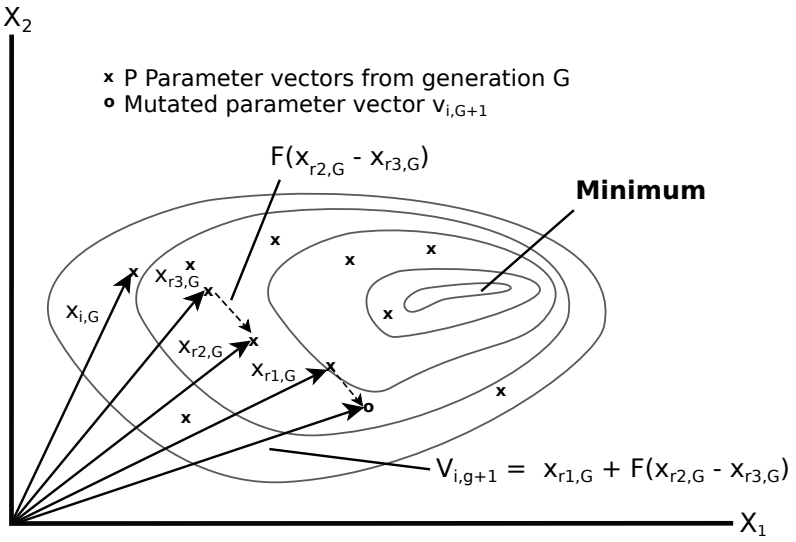

Source: Adapted from Storn e Price (1997).

$$u_{i,G+1} = (u_{1i,G+1}, u_{2i,G+1}, \ldots, u_{Di,G+1}) \tag{5}$$

is formed, where

$$u_{ji,G+1} = \begin{cases} v_{ji,G+1} & \text{if } rand(j) \leq C \text{ or } j = rnbr(i) \\ x_{ji,G} & \text{if } rand(j) > C \text{ and } j \neq rnbr(i) \end{cases} \tag{6}$$

for $j = \{1, 2, \ldots, D\}$. $rand(j)$ is the j-th evaluation of a uniform random number with outcome $in[0, 1]$, and C is the crossover constant $in[0, 1]$ which is determined by the user. $rnbr(i)$ is a randomly picked index $\in 1, 2, \ldots, D$ which ensures that $u_{ji,G+1}$ get at least one parameter from $v_{ji,G+1}$. Figure 6 shows an example of crossover using 7-dimensional vectors. Then, we use a greedy criterion to decide whether it should become a member of generation $G + 1$. If the trial vector $u_{ji,G+1}$ has a lower cost function than the target vector $x_{i,G}$, then $x_{i,G+1}$ is set to $u_{i,G+1}$; otherwise, the old value $x_{i,G}$ is retained.

2.3 Seismic events

Once the acquisition process records the reflection of sound waves, it is essential to understand how sound waves propagate. This section will give the main concepts behind the propagation of mechanical waves, its data representation, and how the reflection occurs.

Figure 6 – Illustration of the crossover process for $D = 7$ parameters.

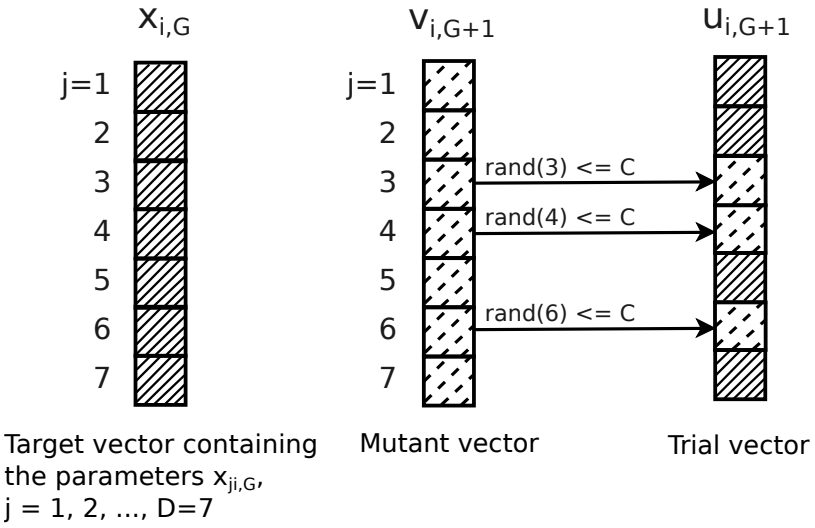

Source: Adapted from Storn e Price (1997).

2.3.1 Seismic wavelet

Mechanical waves can be body waves or surface waves. Body waves are those able to propagate through the interior of a material, while surface waves propagate near the free surface. The sound wave is the only mechanical body wave able to exist in a fluid. In an elastic isotropic solid[1] two wave types are possible: compressional (P) and shear (S). As a mechanical wave propagates, it travels in a particular direction, the transported energy direction. This wave causes a vibration in the material, and the orientation of this vibration is called the direction of particle motion (LINER, 2016). There are two kinds of pure waves: longitudinal and transverse. A longitudinal wave's particle motion is parallel to the propagation direction. The sound and the seismic P-waves are in this category. In a transverse wave, the particle motion is perpendicular to the propagation direction. The seismic S-wave is one example of this kind of wave. Figure 7 illustrates both waves.

A wave propagating through a solid or fluid has a distinct velocity. The material is heterogeneous if the wave speed depends on the observation's point, which is usually the case for seismic body waves where the rocks and pore fluids vary at each point in the earth. The seismic wave speed varies following the temperature, pressure, lithology, and so on (LINER, 2016). Using this description of mechanical waves, we can represent the wave movement over a cartesian plane. The pressure now is a function of x, representing the traveled distance, and will vary between high and low as indicated by Figure 8. The deflection of the wave from zero is called amplitude and represents a physical quantity, in this case, the pressure. In the seismic context, to measure the wave's pressure in function

[1] Isotropic materials - Materials whose properties are independent of the direction of examination (MARSH; RODRíGUEZ-REINOSO, 2006).

Figure 7 – Mechanical waves are distinguished by the vibration pattern caused in the medium. A longitudinal wave (top right) has a particle motion parallel to the direction of propagation, while a transverse wave (bottom right) has a particle motion perpendicular to the propagation direction.

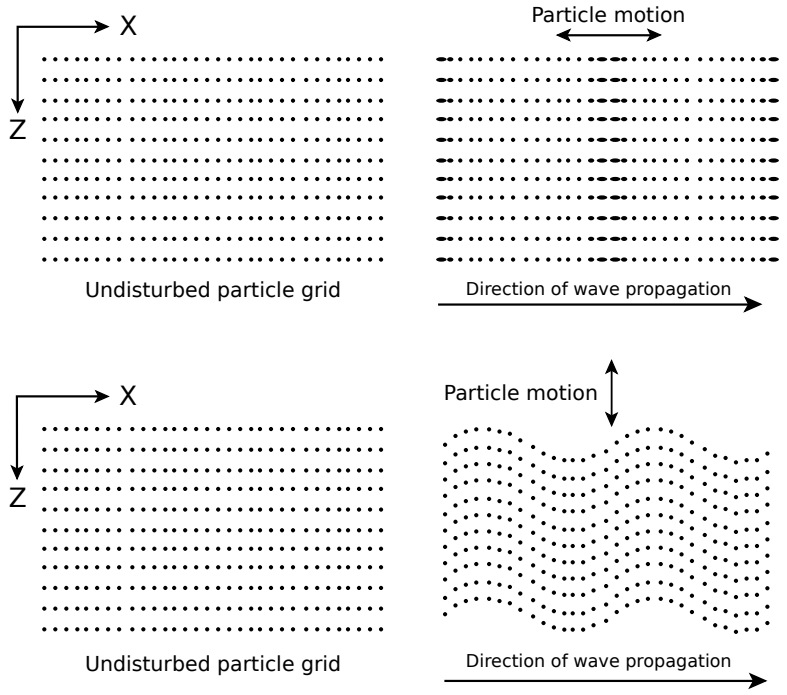

Source: Liner (2016, p. 4)

of time, the receivers are spatially fixed (LINER, 2016).

Mathematically, we can think of a wavelet as built by the sum of multiple cosine curves. The equation for one cosine curve is

$$\cos\_\text{curve}(f, t) = \cos(2\pi f t)$$

where f is the frequency in Hertz and t is time in seconds. In the context of seismic data, we deal with wavelets (or seismic pulses). A wavelet contains many frequencies and is time-limited, meaning that the wavelet only exists for a finite time instead of oscillating forever. Because each frequency has its period (distance between peak to peak), we refer to the entire waveform as having a dominant frequency. The simplest way to estimate the dominant frequency of a seismic pulse is by the maxima frequency of the interest region's frequency spectra (LINER, 2016).

A real seismic wavelet, in general, would have a dominant frequency of around 30-40 Hz. Each cosine curve that compounds the wavelet also has a frequency-dependent phase factor $\phi(f)$ and a peak-amplitude factor $A(f)$,

Figure 8 – Example of seismic wavelet with multiple frequencies characterized by its dominant frequency.

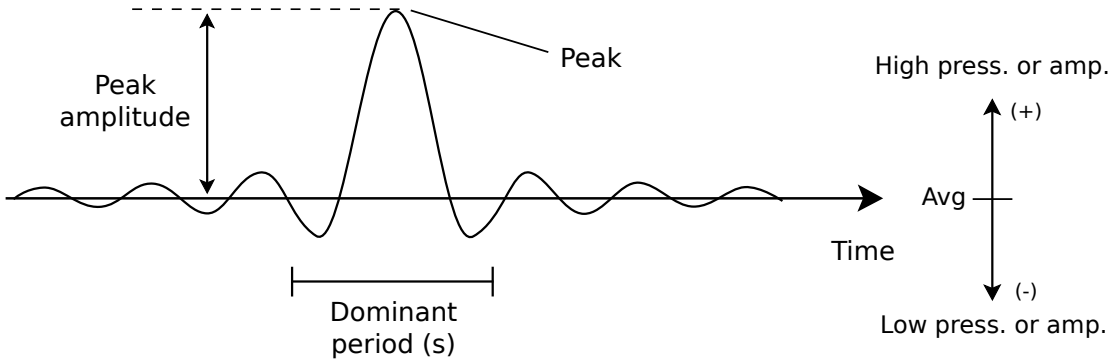

Source: Liner (2016, p. 9)

$$\cos\_\text{curve}(f,t) = A(f)\cos[2\pi f t + \phi(f)] \tag{7}$$

for interpretation, a zero-phase wavelet is preferred because:

1. It is strongly peaked in the sense that side lobes are minimized.
2. It is symmetrical, optimum for vertical resolution.
3. The peak is located at the center of the wavelet.

If the phase of a wavelet is unknown, it can be estimated from a Vertical Seismic Profile (VSP), a synthetic seismogram, or through statistical analysis of the data itself.

2.3.2 Reflectivity coefficient

Reflections arise because of changes in seismic velocity, rock density, or both. Consider a simple model with some layers of rocks where a sound wave is sent downward into the earth by an explosion or vibratory disturbance. In case these waves encounter a discontinuity in acoustic impedance, this results in a reflected wave (Figure 9) (LINES; NEWRICK, 2004).

The acoustic impedance is defined by $I = \rho V$, where ρ is the density and V is the velocity log. The ratio between the reflection amplitude and incident wave is called the reflection coefficient. By solving the boundary conditions for layer discontinuities for an acoustic wave at vertical incidence, the reflection coefficient can be described as

$$R = \frac{I_2 - I_1}{I_2 + I_1} \tag{8}$$

Figure 9 – Reflected and transmitted waves from an incident wave.

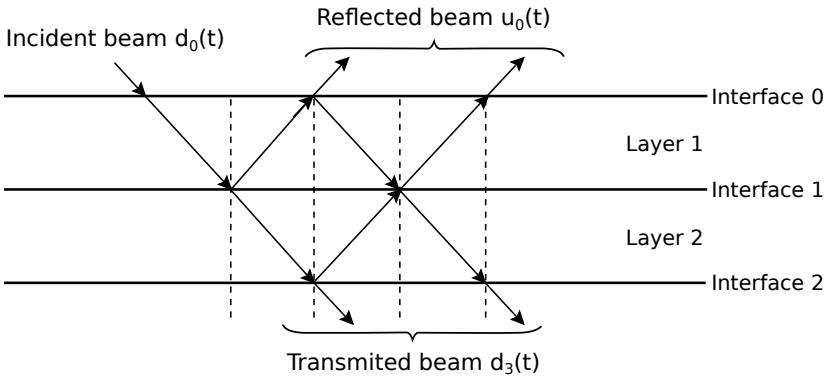

Source: Adapted from Lines e Newrick (2004, p. 36).

where I_1 and I_2 are the first and second layer impedance, respectively. Figure 9 illustrates this process. Generally, a series of reflection coefficients in the depth domain is constructed and resampled in the two-way time domain, corresponding to the travel time of the incident wave to the interface plus the travel time from the interface to the receivers.

2.3.3 Display of wavefield data

When a receiver records data, the created time series consists of consecutive measurements separated by a constant delay (time sample rate). A time series recorded by a seismic receiver is called a trace and, typically, is composed of a few thousand samples with a time sample of 1, 2, or 4 milliseconds. A set of seismic traces forms a seismic gather or section. Usually, we display seismic waves in two forms, as an image or *wiggle trace* (Figure 10). In an image, colors, or gray levels, are associated with the amplitude of the seismic wavelet measured by the receivers. This work will use only a pair of seismic traces (synthetic and observed) represented as a wiggle trace, allowing the interpreter to analyze each trace wave's shape.

2.4 Well to seismic tie procedure

This section will cover the core activity of this work, the well-tie process. This step is crucial for understanding the surface geological structures. It begins by providing a detailed explanation of Well logs and their transformations, followed by the convolutional model. The mathematical model used to construct synthetic seismograms. The process of tying will then be detailed, considering the computation context. Lastly, we will address the importance of quality control and how these constraints impact the tying process.

Figure 10 – Seismic image (a) and *Wiggle trace* (b) of Well F. We shifted the original depth and time.

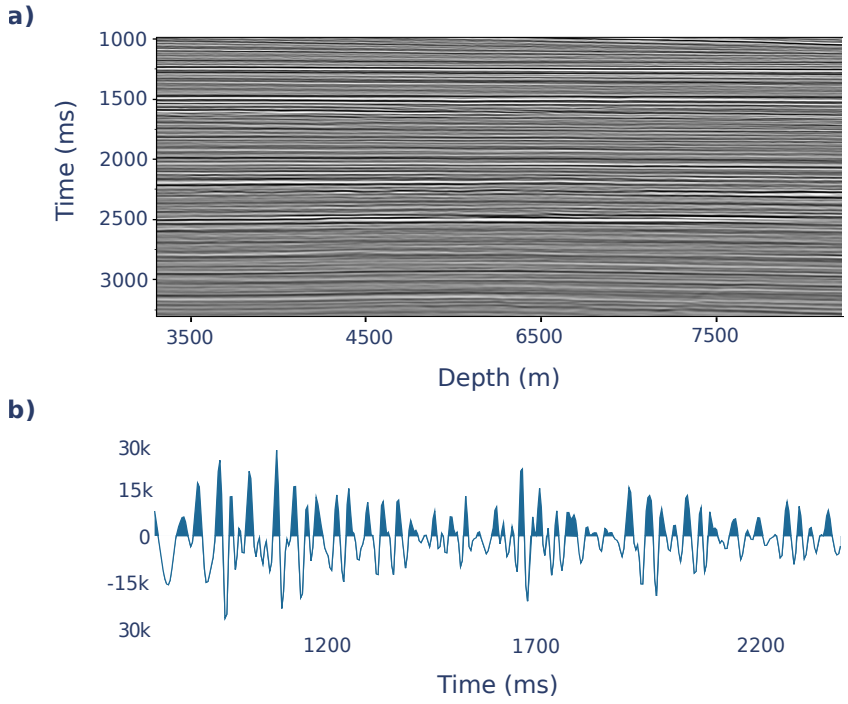

Source: Author

2.4.1 Well Logs

The interpretation requires an Earth model, which consists of physical properties that influence seismic wave propagation. A well is a set of logs, a time series of physical phenomena measured at the same sample domain, the depth. Once a wellbore is not drilled perfectly at vertical, we have two depth measurements: the Measured Depth (MD) measured along the path of the borehole, and the True Vertical Depth (TVD), the absolute vertical distance between the reference (the Rotary Table[2]) and the wellbore. This work uses True Vertical Depth Sub Sea (TVDSS), the vertical depth of the well minus the elevation above the mean sea level.

For the acoustic earth model, the physical properties influence seismic wave propagation. These properties include compressional wave (P-wave) speed and mass density. The cores of 1D seismic are the well's logs calibration, the synthetic seismogram creation, and the conversion of depth into time travel. If a VSP is available for a particular well, is almost known the time-depth relationship. Once it gives a direct measurement of time, depth, and waveform (LINER, 2016).

A VSP is a measurement where a seismic signal, generated at the surface, is recorded

[2] Rotary Table - The revolving or spinning section of the drill floor that provides power to turn the drill string. Source: <https://glossary.slb.com/en/>, access on 26th April 2023.

by geophones (receivers) positioned along the wall of a drilled well. A standard VSP shooting can be categorized into zero-offset and offset VSP. Zero-offset recording surveys have the source localized at the borehole, as shown in Figure 11 (left). While the source of the offset VSP is positioned at a significant distance from the borehole, Figure 11 (right). A check-shot survey differs from a zero-offset VSP for the receiver spacing and data acquired. The VSP gives us a table that relates the depth with the seismic signal travel time, used to tie seismic with the well and calibrate velocity profiles (LINES; NEWRICK, 2004).

Figure 11 – Illustration of a zero-offset VSP or check-shot survey (left), and a far offset VSP acquisition (right).

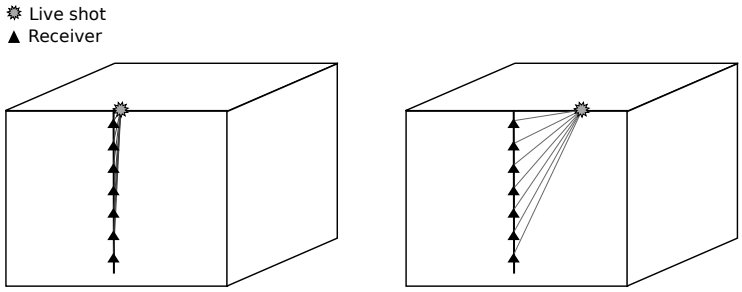

Source: Adapted from Lines e Newrick (2004).

When the check-shot is unavailable, an alternative is to create a synthetic seismogram to convert a sonic log to time and velocity, then directly overlay on the seismic data. To create a seismic trace that theoretically would be recorded at the well's location from the logs, we made some assumptions:

1. The source and receiver are coincident at the Well location;
2. The wellbore is vertical;
3. Velocity, density, and depth log readings are accurate;
4. The velocity field varies only with depth.

A $V(z)$ velocity model is needed to create a synthetic or convert a well log from depth to time. Usually, this velocity is obtained using the sonic log and check-shots. A sonic log typically operates with a depth sampling rate of 0.1524 m. The measured quantity in a sonic log is the reciprocal velocity (slowness) in microseconds per foot (μs/ft), which can be converted to velocity

$$V(\text{m/s}) = \frac{304,800}{\text{sonic}(\mu\text{s/ft})} \tag{9}$$

The check shot can correct any drift due to missing log intervals or any measurement problems that could occur in the acquisition process of the velocity record. Check shots make the calculated travel time more reliable but are often unavailable. Due to the assumption of zero-offset - the source and receiver are in the same position - the general relationship for travel time is

$$\text{time} = \frac{\text{distance}}{\text{velocity}} = \frac{d_1}{v_1} + \frac{d_2}{v_2} + \frac{d_3}{v_3} + \ldots,$$

the second form allows for breaking the distance into constant-velocity segments. From the coefficient reflection theory, subsection 2.3.2, we know that the travel time of a vertical seismic wave for the first layer will be

$$t_1 = 2h_1/v_1$$

where h_1 is the thickness of layer 1, and its velocity is v_1. To calculate the reflection time from interface 2, we segment the distance into two parts

$$t_2 = 2h_1/v_1 + 2h_2/v_2 = t_1 + 2h_2/v_2$$

The last form shows we need to find t_1 only once and reuse it for calculating t_2. Mathematically, this is a recursion, and we can easily extend it to the general case of reflection from n-th interface:

$$t(n) = t_{n-1} + 2h_n/v_n \tag{10}$$

In this way, is associated a reflection time with each interface. We have already established the vital relationship between the geological depth and the seismic travel time. The Equation 10 allows us to estimate a conversion time-depth table for a specific Well through its velocity log, using the sampling rate of the depth log as h and the depth value as n. Where for each velocity log sample at the depth domain, we can estimate its respective time (LINER, 2016).

2.4.2 Convolutional model

The convolutional model is a way to describe the primary reflections as a seismic trace. We can interpret a seismic trace as a series of reflected waves that get at the receivers with different delay times. In other words, the recorded trace is the sum of echoes (LINES; NEWRICK, 2004). Consider the scenario similar to Figure 9, subsection 2.3.2, in which we have a set of three layers of equal travel times, with the two-way traveltimes equal to the sample rate. In this scenario, with two reflecting boundaries, the reflection times series is $\{r_0, r_1\}$. Consider a three-term source wavelet sequence sent down into the earth with amplitudes described by a time series $\{w_0, w_1, w_2\}$. The seismic trace $Y(t)$ is a time series of primary reflections recorded just above the top layer.

The wavelet gives the first sample of the seismic trace reflected off the top layer, which is described by

$$y_0 = w_0 r_0,$$

while the sum of two arrivals gives the second sample, the first wavelet reflected in the second reflector, and the second wavelet value bouncing off the top reflector

$$y_1 = w_0 r_1 + w_1 r_0$$

the third and fourth samples of $y(t)$ are respectively $y_2 = w_1 r_1 + w_2 r_0$ e $y_3 = w_2 r_1$. In this way, the seismic trace is a sum of products. The sum of the subscripts of terms in the series has the same value, which is equal to the index of the trace-sample index. Generally, we can write the time series for the seismic trace in terms of the source wavelet and the reflectivity by the following:

$$y(t) = \sum w_\tau r_{t-\tau}$$

where τ is the summation index representing the propagated waves. This equation describes the discrete convolution process of a source wavelet W with a reflectivity coefficients series R:

$$y(t) = w_t * r_t + n_t \tag{11}$$

where n_t is the noise present in the acquisition process of velocity, density, and seismic pulse estimation.

This model simplifies physical events present in the propagation of seismic pulses, which for this work is good enough (MARGRAVE, 2013). Also, the seismic pulse used in this model can be chosen ad hoc or estimated from the data using any estimation model (CUI; MARGRAVE, 2014). Note that the reflection log is created by Equation 8 at the depth domain, but the convolution occurs at the seismic domain (time), making it necessary to resample the reflection coefficients to the time domain using a time-depth table obtained from velocity log.

2.4.3 Tying the synthetic seismogram with the observed seismogram

The well-tie process used in this work is based on the good practices for the manual tying process defined by White e Simm (2003). Figure 12 shows the workflow composed of three core routines: Well logs edition and calibration, construction of the synthetic seismogram, and the match between the synthetic and observed seismogram. Gray procedures will be detailed in Chapter 4 and comprehend the contributions of this work. Using the presented workflow as a reference, each one of the core routines will be detailed.

Figure 12 – Well-tie process workflow used in this work, gray procedures comprehend the contributions of this work.

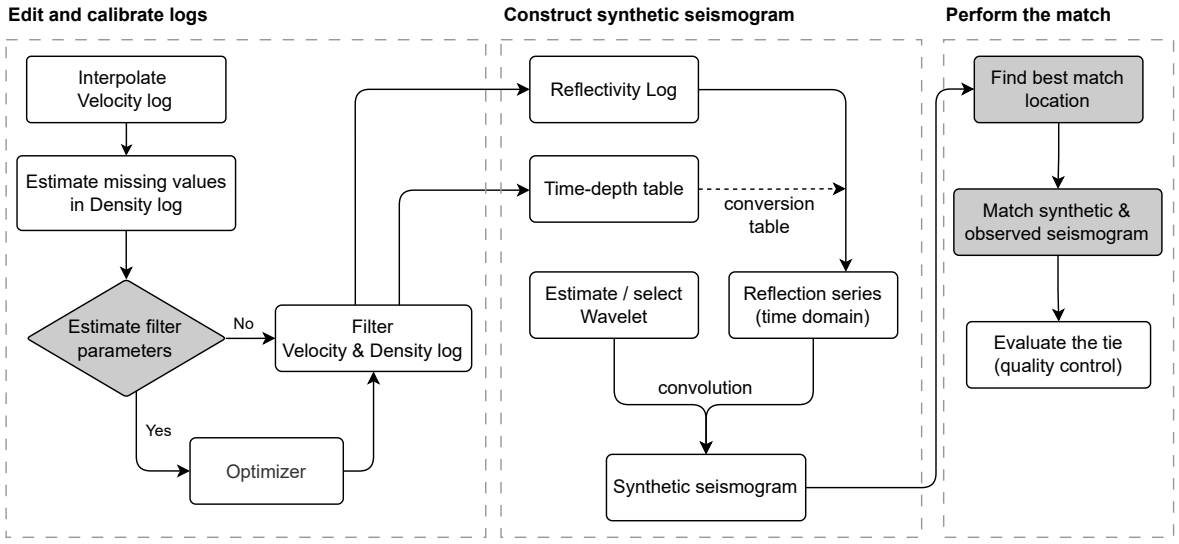

Source: Author

2.4.3.1 Edition and calibration of Well logs

The first step in the tying workflow is the edition and calibration of well logs. This step prepares the data to construct the synthetic seismogram. Usually, the sonic log (slowness) is the reference log during the edition and calibration step. The edition consists of cropping the log to remove spurious measurements, usually present at the start and end. For example, offshore wells (localized at sea) have missing values in their top region (close to the bottom of the sea). This way, constructing a good time-depth table needs to interpolate this region. The cropping prevents unrealistic velocities generation at this region.

Considering the wave propagation mean velocity in the water and near the earth's surface - $\approx$ 1500 m/s and $\approx$ 1700 m/s, respectively - a linear interpolation connects the earth's surface and the first velocity log sample. The size of the interpolated region varies from well to well. This interpolation is the first estimation of the seismogram's match position. The integrated two-way time of the interpolated region estimates the time position (at the seismic log) of the first velocity log sample. Also, a VSP correction in the velocity log can be made after the interpolation to increase the estimated time position accuracy.

When the correct time position of the well top region (first sample) of the well is known, we can apply a bulk shift. A bulk shift means applying a time shift in the synthetic trace by modifying by increasing or decreasing the velocity log in the interpolated region. This modification can also be made directly in the time-depth table - the velocity log and the time-depth table are equivalent by Equation 10. After the interpolation and bulk shift, missing values in the density log are estimated from the velocity log using Gardner's

equation (GARDNER; GARDNER; GREGORY, 1974):

$$\rho(z) = 0.31\mathrm{Vp}(z)^{0.25} \tag{12}$$

where ρ is the bulk density in g/cm^3 and Vp is the P-wave velocity in m/s, both at depth z. With both logs complete, two filters are applied, one to remove spikes (spurious values) and another to smooth the logs. Both filter size and initial bulk shift are hyperparameters defined by the user. In this work, by default, despike and smooth filter sizes are 51 samples and not applied bulk shift. However, in parallel, an optimization approach is used to estimate these values automatically.

2.4.3.2 Synthetic seismogram construction

The construction of the synthetic seismogram is well established (subsection 2.4.2) and has been necessary for the Reflection series, time-depth table, and wavelet. The time-depth table provides tuples (depth, time) associating each Well log sample with one two-way time value. This table converts the primary reflection coefficients (subsection 2.3.2) into the Reflection series, the reflection coefficient resampled in the time domain. Finally, the specialist can select the wavelet ad hoc or estimate from the seismic and well data.

Yi et al. (2013) compared four wavelet estimation methods: (1) estimation from seafloor signal; (2) estimation from Well-log data; (3) statistical estimation from seismic and Well-log data; and (4) estimation as part of sparse-spike deconvolution. The wavelets estimated presented similar results. Simple methods can be as effective as estimated from more computationally rigorous methods. However, each method has different characteristics that may give different results. The best method needs to be determined based on the data and the activity, e.g., well tie or seismic inversion (CUI; MARGRAVE, 2014).

On the other hand, the Ricker wavelets have been empirically successfully used in processing seismic signals (GHOLAMY; KREINOVICH, 2014). The Ricker wavelet is defined, in the time domain, as

$$W(t) = \left(1 - \frac{1}{2}f_p^2 t^2\right) \exp\left(-\frac{1}{4}f_p^2 t^2\right) \tag{13}$$

where t is time, in seconds, and f_p is the most energetic frequency, in radians per second (WANG, 2015). Once the focus of this work is not the wavelet estimation, and our workflow is agnostic to the wavelet used, the Ricker wavelet will default to all the experiments.

2.4.3.3 Matching the synthetic and observed seismograms

Before matching the synthetic with the seismic data, defining the region of the seismic trace where the synthetic log will be associated is necessary. In general, the Well depth is

shorter than the seismic acquisition. For example, the seismic trace in our set of wells has around 8 seconds, while the synthetic log only has 3.5 seconds (including the interpolated top region). This difference in duration means that when working with offshore well-to-seismic tying, the time location of the synthetic log in the observed seismogram is unknown. The matching region is identified by experience, know-how about borehole drilling, and intuition for the manual tie process. White e Simm (2003) find the best match location by scanning the region near the well using a $\approx 500ms$ segment of the synthetic seismogram. The location with the better tie evaluation is considered the correct one.

The tying process aims to match the synthetic seismogram with the observed seismogram to correlate the well's data (the logs) with the seismic data. However, as mentioned before, the well-tie does not aim for a perfect match between the wave shape of both signals but identifies the reflector present at the seismic session that also is present at the Well (NEWRICK, 2012). The time-depth table represents this relationship. Ideally, a good tie does not use stretch and squeeze operations in the synthetic log, relaying only in high-quality logs, calibrating the velocity log with a check-shot or VSP series, and making a good wavelet estimation at the match position. Stretch and squeeze operations can produce non-realistic variations at the velocity log - modifications at the time-depth table are propagated to the velocity log, and vice-versa (WHITE; SIMM, 2003).

However, VSP and high-quality logs are not always available, limiting the applicability of this approach. Motivating an automated or semi-automated, tying approaches that apply stretch and squeeze with constraints to mitigate its effect at the Velocity log (HERRERA; BAAN, 2014; CUI; MARGRAVE, 2014; WANG; LOMASK; SEGOVIA, 2017; WU et al., 2022). On the other hand, we also have approaches that directly modify the velocity log to re-create a synthetic log close enough to the seismogram (GELPI; PÉREZ; VELIS, 2020). Naturally, the perturbations applied in the velocity log are constrained. Reasonable quality control is keeping the velocity variation - compared with the original version - less than 20% (HERRERA; BAAN, 2014).

Chapter 3

Related Work

This chapter will describe various approaches to a well-seismic tie, two semi-automatic tie methods, an automatic tie approach, and one partial seismic-to-well tie automation. The first method is based on DTW to match synthetic and seismic traces and relies on human intervention to verify the quality control. The second approach incorporates quality control, but the execution flow of the method relies on expert interpretation. The third method offers a completely automated workflow, making it the core method of this work, but it needs to improve performance in the proposed wells. Finally, we describe the partial tie process automation, similar to our work, but focused on solving the wavelet extraction problem with neural networks and fine-tuning the workflow parameters using Bayesian Optimization (BO).

3.1 Well to seismic tie with Constrained DTW

The work of Herrera e Baan (2014) was one of the first methods to employ the DTW technique for automatically aligning both observed and synthetic seismic traces using stretch and squeeze operations. The Pearson correlation is the most common metric to evaluate the produced alignment. In addition, a Quality Control (QC) step is employed to mitigate unrealistic distortions by monitoring the velocity variations produced during the alignment process.

DTW is designed to accommodate stretch and squeeze operations in time series by utilizing dynamic programming and considering an initial metric, usually the Euclidean Distance, allowing the construction of a nonlinear alignment between two times series. The DTW distance is the accumulated sum of the distance between a pair of samples along the minimum path in a matrix. Figure 13 shows the distortion path $W = (w_1, w_2, ..., w_k)$

that aligns the elements of the series S and T, minimizing the distance between the two sequences. Aiming to avoid deforming the original time series, a Sakoe-Chiba constraint window is applied.

Figure 13 – Warping path at the minimum distance of two sequences. The dashed lines represent the constraint lines for a warping window with width r.

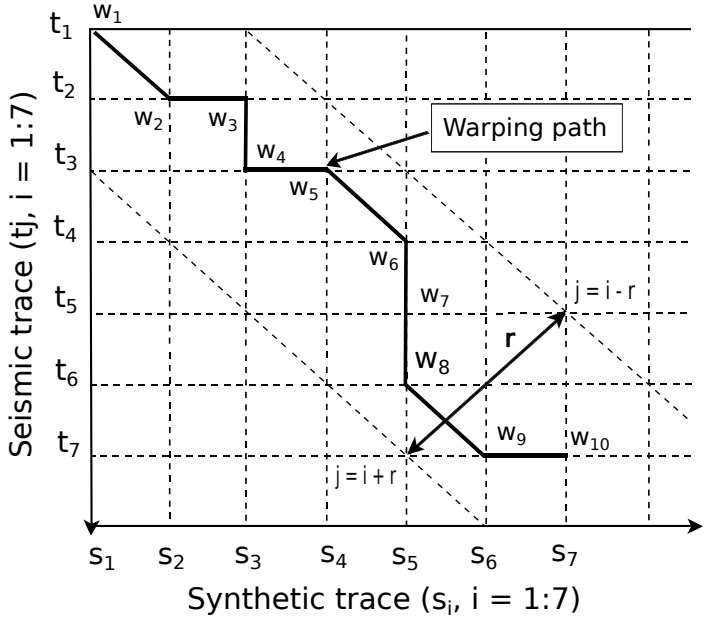

Source: Adapted from Herrera e Baan (2014).

In this matrix, the square distance δ of elements (i, j) are calculated by

$$\delta(s_i, t_j) = (s_i - t_j)^2 \tag{14}$$

To find the best alignment, retrieving the warping path denoted as W from the distance matrix that minimizes the accumulated distance is necessary. We can express this path with the optimal cost as:

$$W(S, T) = \min_{W} \sum_{k=1}^{p} \delta(w_k) \tag{15}$$

where each w_k correspond to the point $(i, j)_k$, and each matrix cell (i, j) represents the alignment between the samples s_i and t_j. The DTW employs dynamic programming techniques to find the optimal path recursively:

$$\gamma(i, j) = \delta(s_i, t_j) + \min[\gamma(i-1, j), \gamma(i-1, j-1), \gamma(i, j-1)] \tag{16}$$

where $\delta(s_i, t_j)$ is the distance defined in Equation 14, the accumulated distance $\gamma(i, j)$ is the sum of the current element's distance and the minimum accumulated distance from its three neighboring cells. This way, the lowest accumulated distance possible is saved at

the last cell of the γ matrix. Traversing in the reverse accumulation order can reconstruct its correspondent accumulation path.

This process warps both time series (observed and synthetic traces), producing two series with length p. Once the tying process does not want to make distortions in the observed trace, is computed a new index argument $\hat{i}$ extracts the indices from the intersections of two sets, $\{i_k\}$ e $\{j_k\}$:

$$\hat{i} = i_k(j_p), j_p \subseteq \text{ position of } \{j_k\} \text{ in } \{i_k\} \cap \{j_k\} \tag{17}$$

In the example shown in Figure 13, from the warped traces S_k and T_k the new argument $\hat{i} = \{1, 3, 4, 5, 5, 5, 7\}$. Using $\hat{i}$ is obtained the trace $S_{\hat{i}}$, which represents the best approximation of the signal T_j. In other words, the argument $S_{\hat{i}}$ accelerates or decelerates the synthetic trace to align it with the observed seismic trace. The Sakoe-Chiba window is employed to reduce the occurrence of nonphysical warping by restricting the maximum allowed distortions of stretch and squeeze applied at the synthetic trace. The window is defined as $|i_k - j_k| < r$, also in Figure 13. Oversampling both traces two or three times can smooth out the time shifts (warping).

As mentioned earlier, the quality control used in the tying process monitors the velocity distortion caused by the path $S_{\hat{i}}$. The rate of change of interval velocity (local) at depth $z_{\hat{i}}$ is given by the derivative of the path $w'(z_{\hat{i}})$ smoothed by the variable $S_{\hat{i}}$, Equation 17. The local velocity change at depth $z_{\hat{i}}$ is

$$V_{P,\text{new}}(z_{\hat{i}}) = \frac{V_{P,\text{old}}(z_i)}{w'(z_{\hat{i}})} \tag{18}$$

while the new time-depth curve is obtained from

$$t_{d,\text{new}}(z_{\hat{i}}) = 2 \sum_{k=1}^{\hat{i}} \frac{\Delta z_k}{V_{P,\text{new}}(z_k)} \tag{19}$$

The *Constrained* DTW approach has been evaluated by comparison with a manual tie approach. Figure 14 shows the evaluation. The manual tie was conducted following the best practices presented by White e Simm (2003), resulting in a correlation coefficient of 0.80. Through experiments using the *Constrained* DTW approach, the author achieved a correlation of 0.89 using a Sakoe-Chiba window with $r = 10$ samples at a sampling rate of 2 ms. This window implies that peaks can be considered the equivalent if they are within a 20 ms range. However, when using a larger window size, $r = 20$, there was an increase in the correlation to 0.92, but the velocity profile has a distortion of 40%, higher than the maximum allowed.

In summary, the experiments presented by Herrera e Baan (2014) demonstrate the method's capacity to construct an alignment more correlated than a manual approach. The main feature of the proposed approach is to use a constraint window to reduce nonphysical alignments. The window limits the amount of warping used in the synthetic

Figure 14 – Performance comparison between *contrained* DTW and manual tie. (a) Manual tie with a correlation of 0.80. (b) Automatic tie with $r = 10$ and correlation of 0.89. (c) Automatic tie with $r = 20$ and correlation of 0.92. (d) The ratio of relative velocity change using different window sizes in the automatic tie.

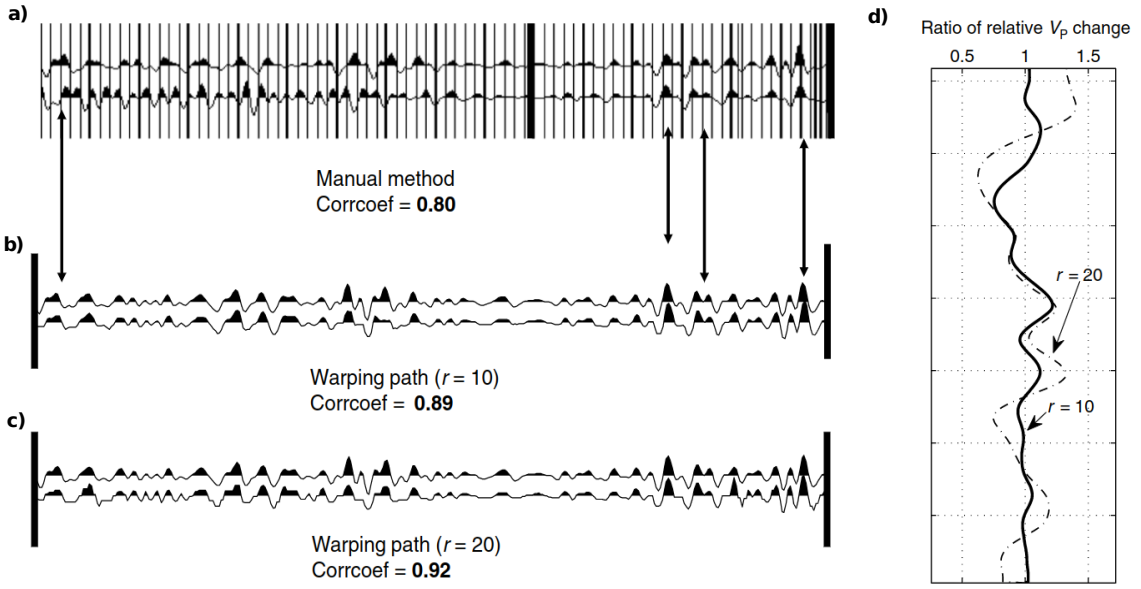

Source: Adapted from Herrera e Baan (2014).

trace. However, it is necessary to verify the alignment validation by checking the ratio of relative V_p change because, during the construction of the DTW warp path, we do not control the distortions caused in the velocity profile. If the alignment provides a distortion higher than allowed, a new alignment needs to be performed using a window size shorter than before, turning this into a semiautomatic well-to-seismic tie approach.

3.2 Geological Layer-Constrained Seismic-Well Tie through Blocked Dynamic Warping

The principal limitation of applying DTW algorithm to tie seismic and well data automatically is the tendency to generate geologically unrealistic velocities. To overcome this limitation, Wang, Lomask e Segovia (2017) proposed the *Blocked Dynamic Warping* (BDW) algorithm, which can achieve an optimal tie consistent with the geological constraints of velocity. BDW apply linear or constant velocity variations constrained in blocks, typically representing geological layers.

Several modifications are made compared to *contrained* DTW. Firstly, the data domain on which the DTW algorithm is applied changes. Instead of directly warping the synthetic seismogram's sample index, BDW aims to estimate a series of time shifts applied to the synthetic trace to minimize its distance to the observed seismogram. Mathemati-

cally expressed as follows:

$$\min_{\tau \in R^n} \sum_{i=1}^{N} (S(i) - Q(i + \tau(i)))^2 \tag{20}$$

where S and Q represent, respectively the observed and synthetic seismogram, τ is a vector of shifts to be applied to trace Q, R^n is an n-dimensional space in the real numbers. Since the traces S and Q may not have the same length, we can use an extrapolation for the regions where the shifted time falls outside the range of Q.

The process of solving this optimization problem using dynamic programming occurs analogously to the one presented in the previous section:

$$\gamma(i, \tau_i) = \delta(i, i + \tau_i) + \min[\gamma(i - 1, \tau_i - 1), \gamma(i - 1, \tau_i), \gamma(i - 1, \tau_i + 1)] \tag{21}$$

where $\tau_i = \tau(i)$ is the shift of the i-th sample, $\gamma(i, \tau_i)$ is the accumulated error, and $\delta(i, i + \tau_i)$ is the matching error between the i-th sample of the first sequence (usually the seismic log) and the $(i + \tau_i)$-th sample of the second sequence (usually the synthetic log). The interpreter can define a block scheme with various size and velocity models. Suppose there are a total of m blocks bounded in the time domain $\{t_0 = 0, t_1, t_2, ..., t_m = T\}$, discretizing the Equation 20:

$$\min_{\tau \in F_m} \sum_{i=1}^{N} (S(i) - Q(i + \tau(i)))^2 \tag{22}$$

By changing the warping path function from an n-dimensional space to F_m, the product of m space functions, where m represents the number of blocks. We define each of the m space functions according to the chosen velocity model. These models are assigned based on geological interpretation, Wang, Lomask e Segovia (2017) present two velocity models: the constant and the linear variation models.

In the constant variation model, the velocities within each block vary constantly and are adjusted by adding or subtracting constant values. This procedure is equivalent to specifying that the time shift inside the block is linear. Mathematically, this can be expressed in terms of depth D and travel time t as

$$\frac{d\tau}{dD} = \frac{dD}{d(t + \tau)} - \frac{dD}{dt} \tag{23}$$

where the τ is the time shift.

Sometimes, only the constant model is not enough to represent, for example, the increase of compaction caused by a thicker overburden. In this scenario, one standard and practical approach is to use a linear variation model known as the $V_0 - K$ model. BDW performs this modeling by defining the function through its derivatives. Formally, a constant acceleration above zero can be expressed as

$$\frac{d^2D}{dt^2} = C_0$$

this expression gives the derivative of time concerning the depth for constants C_0 and C_1:

$$\frac{dt}{dD} = \frac{1}{c_0 t + c_1}$$

similarly, we can calculate the derivative of the shifting function τ to depth D as

$$\frac{d\tau}{dD} = \frac{1}{C_0'(t+\tau) + C_1'} - \frac{dt}{dD} \tag{24}$$

This equation calculates the warp path of time sifts from the end of one block to another while maintaining a constant acceleration. In these blocks, the BDW estimate the optimal pair (C_0', C_1'), which represents the optimal time warping. This way, the algorithm can simultaneously calculate both the constant and linear velocity model, so the blocks do not need to have the same types of velocity variation.

In Figure 15, we can visualize the BDW entire workflow to a well-to-seismic tie. The input data includes well logs, including the observed seismogram. The synthetic seismogram is created by calibrating a wavelet and using an initial time-depth curve. Next, with the layer boundary scheme defined, each block must be associated with a velocity model type (constant or linear). It is also possible to assign a permissible velocity range to each block. If the tie is inadequate, we can adjust the number of blocks, their boundaries, the velocity interval, and the type. The remaining steps are the same as *Constrained* DTW approach, involving the error accumulation and warp path construction. Once is achieved a good tie, the time-dept curve and the well logs are updated.

Figure 15 – A complete workflow of BDW.

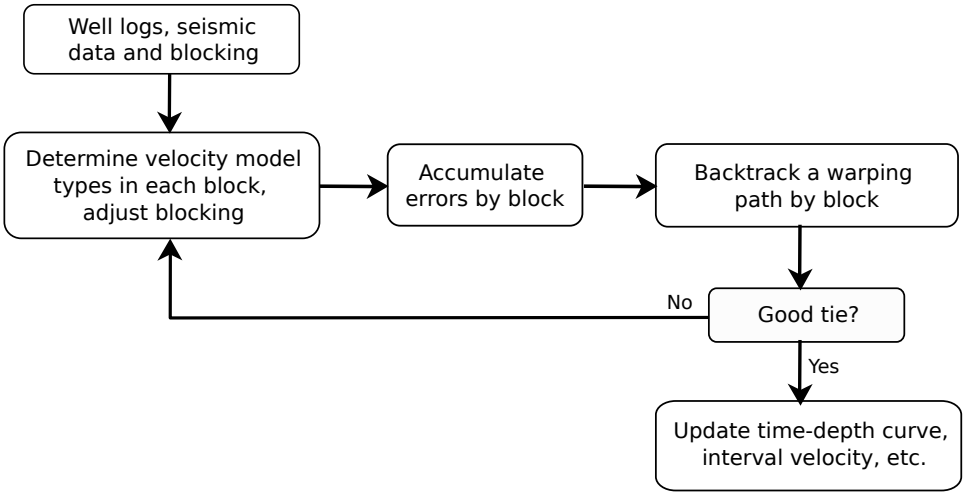

Source: Adapted from Wang, Lomask e Segovia (2017).

Wang, Lomask e Segovia (2017) compared their proposed method with two other methods, the bulk shift using cross-correlation and a DTW approach. The bulk shift

technique shifts the entire synthetic seismogram where the best shift is defined by cross-correlation. The well-seismic tie was performed on a well located in the Norwegian North Sea. A zero-phase wavelet was extracted from the observed seismogram, and the well logs were processed to estimate regions with missing data. Both synthetic and observed seismograms were normalized. Finally, the blocks were defined based on the check-shot profile. The three methods obtained the following correlations: bulk shift achieved 0.27, DTW 0.73, and BDW 0.67. DTW have achieved a higher correlation than BDW, but the velocity variation was up to 20%. In contrast, the BDW exhibited a more reasonable velocity distortion.

The interpolation was required to calculate the interval velocity or the smoothed time-depth curve using *Constrained* DTW. Increasing the number of blocks used in BDW may be necessary for well ties involving more complex wells. To incorporate this method into an automated tie workflow, it is necessary to automatically segment the velocity profile into blocks and associate a velocity model.

3.3 Automatic well tying and wavelet phase estimation with no waveform stretching or squeezing

By adopting a significantly different approach from previous methods, Gelpi, Pérez e Velis (2020) disturbs the velocity profile directly to create a synthetic trace more similar to the observed seismogram. Furthermore, this approach turns the alignment process into a multimodal optimization task, which enables estimating the wavelet phase during the tie. Finally, the method iteratively applies perturbations to the velocity profile and wavelet phase to enhance the correlation between the synthetic and observed traces.

From the original velocity profile (here called of observed velocity) $V_{\text{obs}}(z_i)$, $i = (1, ..., N)$, the perturbed velocity log is calculated as

$$V_{\text{per}}(z_i) = V_{\text{obs}}(z_i)[1 + p(z_i)] \tag{25}$$

where $p(z_i)$ is a perturbation function obtained through a cubic spline interpolator with M knots, $M \ll N$ and $-P \leq p(z) \leq P$, P is user-defined and represents the maximum perturbation allowed to the velocity profile. The M knots are evenly distributed in the depth domain for simplicity.

In each iteration of the optimization algorithm, is also adjusted the wavelet phase by applying a constant phase rotation using the Hilbert transform:

$$W_{\text{rot}} = \cos(\theta)W_0 + \sin(\theta)H\{W_0\} \tag{26}$$

where θ is an unknown rotation angle, W_0 is a zero-phase wavelet, and $H\{\cdot\}$ is the Hilbert transform. The wavelet can be selected ad hoc or estimated in a practical context. The

author chose to use the Ricker wavelet, commonly used as a standard ad hoc wavelet in the industry (GHOLAMY; KREINOVICH, 2014). Thus, the process of the well-seismic tie is reduced to finding the values of the M knots within the interval $[-P, P]$ and the phase θ that maximizes the correlation coefficient between the synthetic and observed seismic trace. This correlation can be achieved through the minimization of the following cost function:

$$J = 1 - \gamma \tag{27}$$

with γ, $-1 \leq \gamma \leq 1$, being the correlation coefficient between the synthetic, $\hat{S} = (\hat{s}_1, \hat{s}_2, ..., \hat{s}_N)$, and the observed trace, $S = (s_1, s_2, ..., s_N)$. Since J is a nonlinear multimodal function, the global optimization algorithm *Differential Evolution* (DE) is used to find the optimal solution. In each iteration of DE, the knots and wavelet are updated, and the velocity profile and seismic wavelet are modified using Equations 25 and 26. The entire routine of synthetic log construction needs to be executed to calculate the cost function.

To validate the proposed method, Gelpi, Pérez e Velis (2020) conducted two types of experiments. The first used synthetic data to analyze the impact of parameters on the obtained solution, while the second employed real data to compare with a standard DTW approach. Initially, the impact of M was evaluated by running the method with a fixed P of 15% for a different number of knots $M = \{3, 5, 10, 50, 100\}$. As shown in Figure 16, values of M too high increase the instability of the curve $p(z)$, causing abrupt variations in the velocity profile, although still within the range $[-P, P]$ and the synthetic trace exhibits a high correlation coefficient. While using a low M value is insufficient to align the traces.

When the same experiment was done with the number of knots fixed on $M = 10$ and P assuming different values $P = \{5\%, 10\%, 15\%, 20\%\}$, the obtained $p(z)$ curve did not show significant variation with all cases obtaining high correlation. This result indicates that despite the correlation being directly related to the value of P, satisfactory results can be achieved with minimal velocity distortion. A statistical analysis of 100 runs varying the number of knots and maximum perturbation found that when these values are low, the quality of the estimated phase decreases. The insufficient perturbation leads to the assignment of arbitrary values to the phase. Curves obtained from multiple executions with the same configuration were quite similar, but they exhibited instability in the top region of the data.

When applying the approach to data from the Neuquén Basin in Argentina, as shown in Figure 17, the obtained correlation coefficient increased from 0.64 to 0.88, which is a satisfactory result. Furthermore, the optimal phase rotation found was 82°, close to the estimated 90°. As a comparative analysis, were aligned the same data using the *Constrained* DTW (HERRERA; BAAN, 2014), with a window of 10 samples and without

Figure 16 – Pseudo-synthetic example: results with a velocity change of 15% for a different number of knots. (a) Observed velocity (black) and perturbed velocity, (b) $p(z)$ curves, and (c) corresponding synthetic traces.

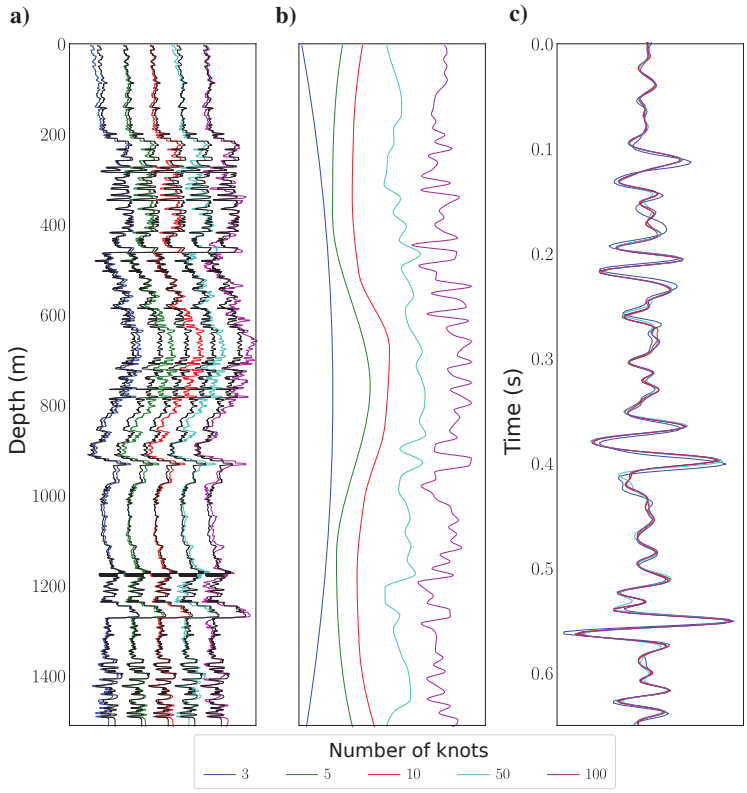

Source: Gelpi, Pérez e Velis (2020)

data oversampling that achieved a correlation of 0.94. However, some undesired and unrealistic features were observed, such as flat and peaky wave lobes. These features do not appear when using the optimization approach.

In summary, the method proposed for Gelpi, Pérez e Velis (2020) can automatically align seismic traces and estimate the wavelet rotation. Using a cubic spline interpolator achieves high control over the velocity distortion. The statistical analysis confirmed the method's robustness, mainly when using moderate parameter settings. Moreover, the method achieved a correlation above 0.7 and acceptable wavelet phases in the experiment's data.

3.4 Partial automation of the seismic to well tie with deep learning and Bayesian optimization

Similar to our work, Tschannen, Ghanim e Ettrich (2022) made automation of the seismic to well tie process using deep learning to make the wavelet extraction and Bayesian search to fine-tune hyper-parameters of the workflow. The wavelet extraction uses a

Figure 17 – Neuquén Basin field data example (well A): (a) observed (black) and perturbed (red) velocity logs, (b) $p(z)$ curve with $M = 15$, $P = 15\%$. (c-e) observed (black) and synthetic seismograms (red) after manual tying, the proposed method, and *Constrained* DTW, respectively.

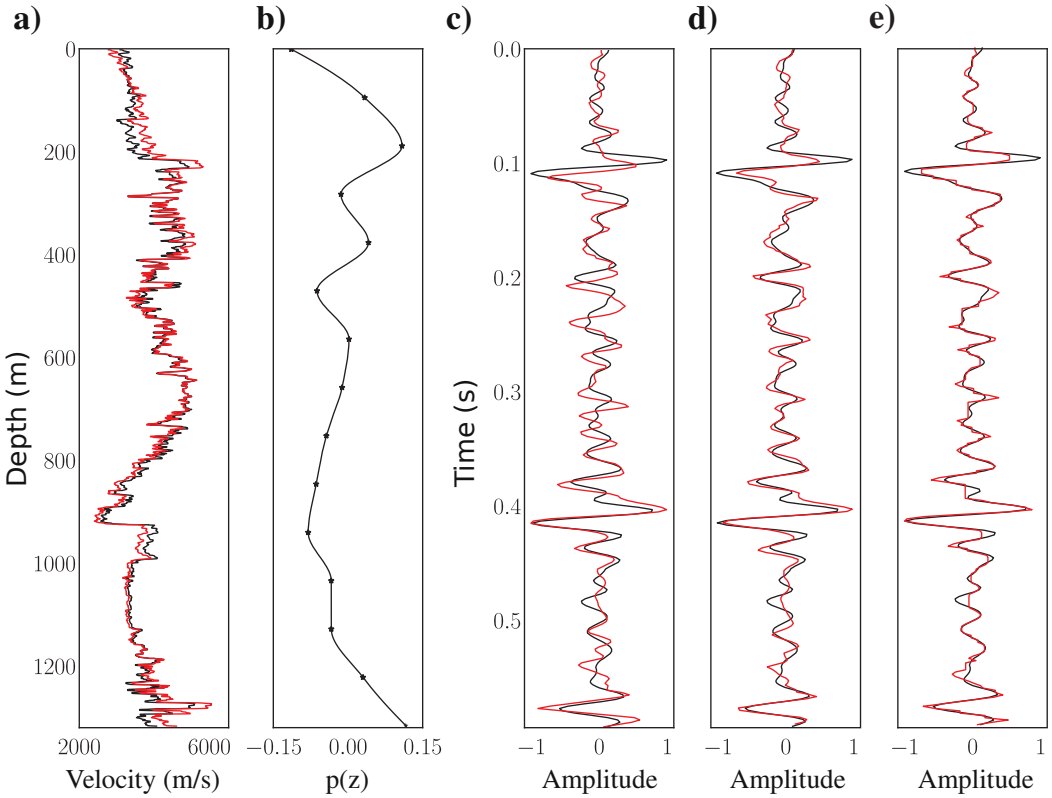

Source: Gelpi, Pérez e Velis (2020)

variational convolutional neural network to learn the deconvolution process and robustly estimate wavelets given input series of arbitrary lengths. The variational nature of the neural network allows for quantifying the uncertainties of the process, in particular, the wavelet phase.

The input data for the well-to-seismic tie approach are the well trajectory, a time-depth relation table, the seismic trace extracted along the well path, and well logs - acoustic velocity, bulk density, and shear velocity to tie in the prestack well. Similar to the workflow described by Simm e Bacon (2014), the main steps to perform the tying can be summarized as (1) convert logs from depth to two-way time domain; (2) compute the reflectivity; (3) extract a wavelet; (4) compute the synthetic seismogram; and (5) evaluate the similarity between the synthetic and observed seismic trace.

Following the convolutional model, already described in section 2.4.2, it is assumed that the seismic trace results from the convolution between the source wavelet and the reflections series. In this way, both the seismic and the reflection series are known. Then, the goal is to solve the inverse problem to estimate the wavelet's shape. At this stage, the timing between the seismic and the reflections is considered correct. The neural network

f_θ and its train parameter θ is designed as

$$f_\theta(S(t), R(t)) = \hat{W}(t) \approx W(t)$$

where S and R, are the seismic and reflection series, W is the wavelet and $\hat{W}$ is the estimated wavelet.

The neural network uses a convolutional variational auto-encoder architecture, as shown in Figure 18. In the first part of the network, a 1-dimensional CNN takes the concatenated seismic and reflection series along a sequence of convolutional and pooling layers after the data passes through a Global Average Pooling (GAP). This layer takes the mean value along the time dimension and outputs a vector with a fixed size equal to the number of filters of the last layer, a hyper-parameter. Consequently, the network supports arbitrary shapes and can operate with traces of variable lengths. In the second step of the neural network, the data is sent to a variational decoder, a standard multi-layer perceptron composed of fully connected layers. However, instead of a deterministic link between the encoder and decoder, a variational formulation imposes a stochastic regularization to map the input data to a zero-centered Gaussian distribution with unit diagonal variance in the latent space.

The network is trained by supervised learning with 150,000 synthetic training samples. Each sample comprises a random source wavelet, random reflectivity, and random noise vector with the corresponding synthetic seismic trace. The network output is a wavelet with 300 ms sampled in 2 ms. The network is trained for 270 epochs with a stochastic momentum gradient descent optimizer with an initial learning rate of 0.003, decreasing

Figure 18 – Simplified overview of the variational auto-encoder used to estimate the seismic wavelet. The black arrows indicate the data flow from left to right during the forward pass.

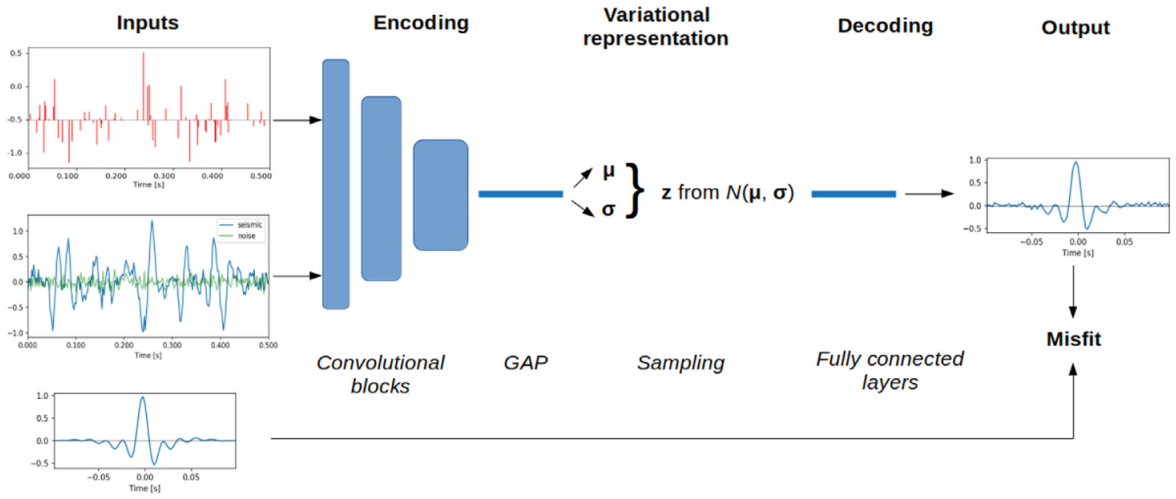

Source: Tschannen, Ghanim e Ettrich (2022).

by 10% every 20 epochs. Mean absolute error is used as wavelet loss to measure the error in the wavelet reconstruction:

$$\text{wavelet loss} = \frac{1}{N_t}\sum_t |\hat{W}(t) - W(t)|$$

where N_t is the number of time samples. It uses a variational loss to measure the statistical distance between the unit Gaussian distribution and the latent distribution, expressed as

$$\text{variational loss} = \frac{1}{2}\sum(1 + \log(\sigma^2) - \mu^2 - \sigma^2)$$

both losses work against each other as the variational term introduces noise, increasing the wavelet loss. To find the balance between both terms is introducing a scalar hyper-parameter $0 \leq \alpha \leq 1$, as shown in Equation 28. Initially, $\alpha = 0.05$ increased until 0.5 with a rate of 10% every 20 epochs. Starting with a small value allows the network to focus first on estimating the wavelet. As α increases, it gives more importance to the regularization term.

$$\text{total loss} = (1 - \alpha) * \text{wavelet loss} + \alpha * \text{variational loss} \tag{28}$$

During the tying process, geoscientists have to adjust some parameters to increase the quality of the tie. Defining a parameter space for each parameter that needs tuning allows a global optimization algorithm to search for the better parameter combination. Bayesian Optimization (BO) is a popular approach to search hyper-parameters of machine learning models due to efficiently tackling the trade-off between exploration and exploitation. Given initial observations, the method builds a surrogate model, a common choice is Gaussian process (GP) regression, that estimates the performance and uncertainties over the entire parameter space. Based on its current estimation, the algorithm relies on an acquisition function to decide which parameters should be evaluated next.

After, the covariance matrix is updated, and until met some convergence criteria the operation is repeated. Here, is used the upper confidence bound to select the following observation. Each point x^* approximated by the GP can be considered as a normal random variable with a mean $\mu[x^*]$ and variance $\sigma[x^*]$, the upper confidence bound equal to:

$$\text{ubc}[x^*] = \mu[x^*] + \beta\alpha[x^*] \tag{29}$$

where β is a positive parameter balancing the two terms. The function will favor regions with considerable expected improvements (exploitation) or higher uncertainties (exploration). It is defined as a simple 4-dimensional parameter space, the first parameters are the well's logs despiking window, constrained into the range of 22 ms and 126 ms, and the despiking threshold, constrained between 0.1 and 5 standard deviations. The third parameter is a Gaussian smoothing kernel's standard deviation, constrained into 0.5 and

5. The final parameter is a time-depth bulk shift between ±12 ms. At each iteration, the goodness of the tie is measured as the central cross-correlation between observed and synthetic seismic traces.

Following Herrera e Baan (2014), the time-depth relationship is corrected based on dynamic time lags between the synthetic and read data. Inspired by DTW, a sliding cross-correlation is used to find the time lag at every trace sample, Figure 19. The window length satisfies a trade-off between smoothness and accuracy, while the maximum lag is an explicit restriction to mitigate unrealistic stretches. Both parameters are selected manually once this process can easily lead to nonphysical modifications. Once the time lags have been found, the time-depth table is updated, and the final seismic wavelet is extracted.

Figure 19 – Example of dynamic lags computed between a real seismic trace (above) and the synthetic one (below). Orange lines represent the local time lag that should be applied to the synthetic trace to increase the overall zero-lag correlation with the real trace.

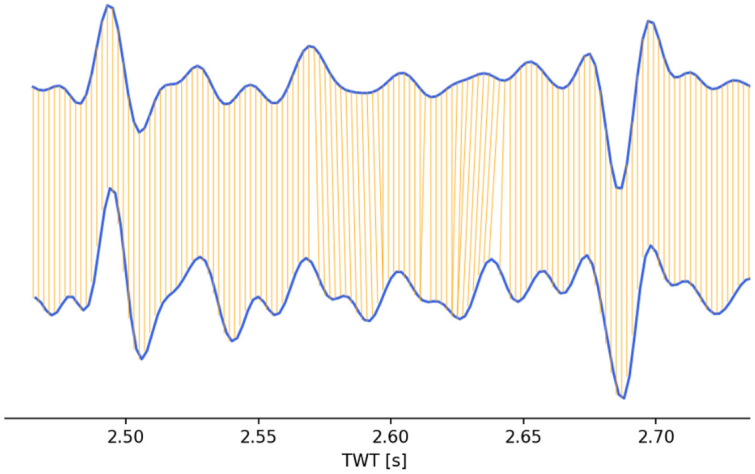

Source: Tschannen, Ghanim e Ettrich (2022).

The proposed method was evaluated on the well Torosa from the Poseidon dataset using an automatic stretch and squeeze with a window length of 60 ms and a maximum lag of 10 ms. The optimized tie exhibits a better fit, and the predicted wavelet shows a more realistic phase. Figure 20 shows both the non-optimized and the final tie. The non-optimized tie of the residual energy shows a misalignment in the spike region of the seismic trace. In the optimized tie, the residual energy is constant throughout the trace and exhibits a random character.

In the second experiment, a prestack well tie was performed on the well 15/9-19 A of the Volve dataset using a methodology similar to the stack well tie. The shear velocity log is also required to compute an angle-dependent reflectivity with Zoeppritz equations in stack well tie. The stretch and squeeze operation was performed using a window of 40

Figure 20 – Tie results for the well Torosa of the Poseidon dataset. AI stands for Acoustic Impedance, and R0 is the vertical incidence reflectivity. Seismic traces are repeated times time to improve visibility. (a) Naive results without parameters fine-tuning, the residual energy shows a slight misalignment in the spike events. (b) Optimized results after stretch and squeeze, the reflectors in the synthetic match the corresponding events almost perfectly.

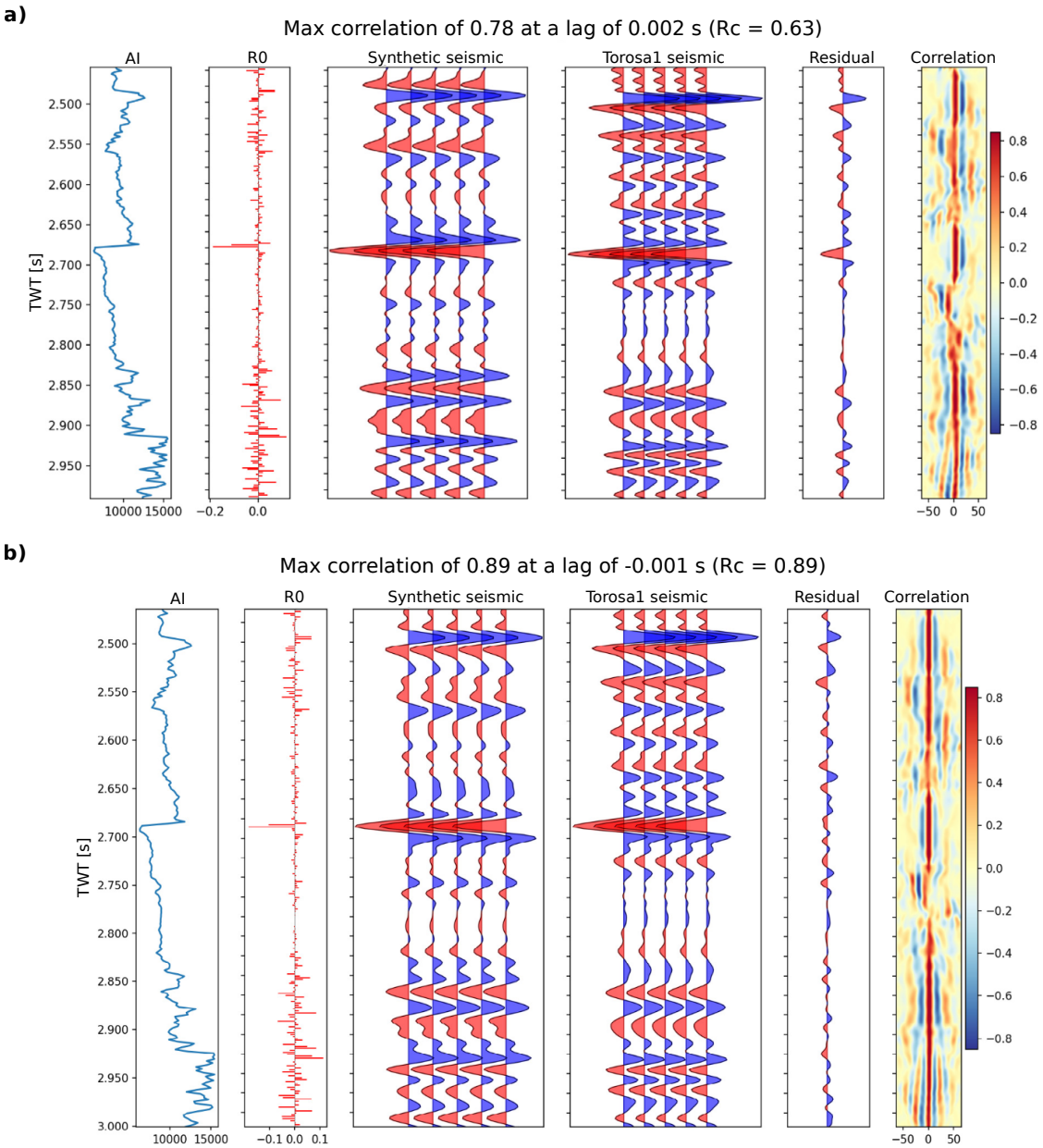

Source: Adapted from Tschannen, Ghanim e Ettrich (2022).

ms and a maximum lag of 8 ms. The semi-automated approach achieved a good result, which is more stable than the tie obtained with a manual approach. When processing noisy data with short extraction windows, the instability of the manual tie requires a time-consuming fine-tuning of various parameters to achieve good results.

The approach proposed by Tschannen, Ghanim e Ettrich (2022) shows that deep lear-

ning and BO are potent methods to automate well tying partially. The neural network is robust to noisy inputs and provides consistent results, and predicts a trustworthy wavelet without resorting to any blocking technique. Introducing the GAP allows arbitrary reflectivity and seismic lengths, while the variational aspect estimates uncertainties in the deconvolution operation. Also, the networks are more stable than traditional methods, and the process of iteratively searching the best parameters can be automated by Bayesian search. The geoscientist can control the optimization by designing the parameter space and bounds.

The work assumes that the seismic and well data are reasonably processed and have a reliable first estimation of the time-depth table. Another limit concerns the poor extrapolation capacities of neural networks. The network's results will likely be wrong if the real wavelet is too different from the synthetic training wavelets. Additionally, automatic stretch and squeeze can overcome minor alignment errors. Still, the method does not use prior geology knowledge, which might lead to erroneous modification in the time-depth table.

3.5 Final Considerations

This chapter presented four approaches to automatically or quasi-automatically matching the synthetic seismic traces, with one partially automating the entire well-tie process. The first two methods use DTW algorithm to find the optimal warping to the synthetic trace but require human intervention to obtain good ties. On the other hand, the third one can obtain similar synthetic traces without human intervention but is focused on well with a short depth length. These three matching approaches have oriented our proposed matching algorithm.

The partial automation of the seismic well-tie procedure can estimate a reliable wavelet and match both traces. However, it is limited to wells with a reliable initial time-depth relationship once finding the matching region is not included in the proposed workflow. The chosen matching approach can easily lead to misalignment requiring human validation, and the neural network has small extrapolation capabilities. The main difference between the automation proposed by Tschannen, Ghanim e Ettrich (2022) and our proposed workflow is the introduction of an algorithm to estimate the matching position, the use of ad hoc wavelet in the construction of synthetic trace, and a reliable matching approach that can obtain good results without human intervention.

Chapter 4

Automatic process for segmented well to seismic tie

This chapter presents our proposed automatic process for segmented well to seismic tie. Our proposed approach can estimate the matching region and automatically match both traces using a segmented strategy of the Gelpi, Pérez e Velis (2020) matching method. First, Bayesian Optimization (BO) estimates the best initial synthetic seismogram parameters. Based on this synthetic trace, DTW algorithm estimates the more probable matching region. With the matching region defined, the seismic trace and well are segmented using the optimal time-depth relation obtained with the *Constrained* DTW. For each segment, DE is used to perturb the velocity log to construct a synthetic trace similar to the real seismic data.

4.1 Estimation of the matching region with DTW

In general, previous works about automatizing the tying process do not include estimating the matching region (HERRERA; BAAN, 2014; WANG; LOMASK; SEGOVIA, 2017; GELPI; PÉREZ; VELIS, 2020; TSCHANNEN; GHANIM; ETTRICH, 2022). However, the matching region is sometimes unavailable, like in our set of wells. This way, the region of the real seismogram corresponding to the synthetic trace needs to be estimated before matching both traces. Figure 21 shows Well A's synthetic and observed seismic trace. The presented synthetic seismogram was constructed by interpolated well logs[1], which comprehends the region until 1.3 seconds and represents the well top's position in the

[1] See the subsection 2.4.3 for more details about how this interpolation process works.

two-way time domain. Once this initial estimation is only based on linear interpolation, its precision decreases as more missing values we have.

Figure 21 – Comparison between the seismic trace with 8.5 seconds (top) and the initial synthetic trace with 3.7 seconds (bottom).

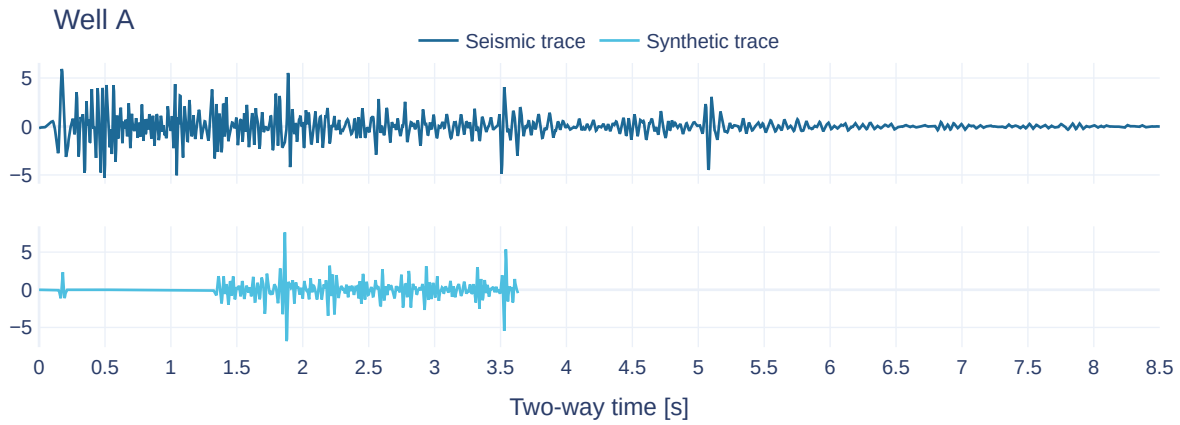

Source: Author

The Munoz e Hale (2012) work is one of the first to aim automatically tying well logs to seismic data using DTW algorithm, fomenting the use of DTW to tying well with seismic data through operations of stretch and squeeze. In this approach, we consider the well-tie problem a subsequence alignment task using the DTW algorithm to align both traces without cropping the observed seismogram, estimating the matching region. However, the work data do not suffer from the attenuation problem described by Margrave (2013) and do not use quality control to monitor the warping effect in the velocity log.

The attenuation effect is time- and frequency-dependent because the propagated wavelet evolves as it propagates, progressively losing high frequencies and undergoing phase rotations (MARGRAVE, 2013). This effect can be easily noticed in Well A's seismogram in Figure 21, where the amplitude and frequency of the top region of the signal are entirely different from the bottom region after 5.5 seconds. On the other hand, the convolutional model considers a static wavelet convolution to construct the synthetic trace. In manual tying, the typical approach is constructing the synthetic trace using a wavelet estimated in the region of interest. The interest region, generally, is localized at the well's bottom and identified as a high amplitude oscillation (pick and valley) in the seismogram, corresponding to a prominent reflector at the bottom of the well.

When applying the Munoz e Hale (2012) approach to estimate the matching region in our wells, we found a tendency to align the synthetic trace in a region deeper than manually annotated. This shift occurs because of the amplitude difference between the seismic trace around 2 seconds and the same region with the synthetic one, which is more similar to the region from 2.5 to 4 seconds. Amplitude differences greatly influence the final alignment once the DTW algorithm's cost function uses the Euclidean distance.

Then, a search region limits the synthetic trace's position to mitigate the shift effect.

The search region is determined based on the maximum velocity perturbation allowed, so positioning the synthetic trace outside this region requires perturbing the velocity above the maximum allowed. Figure 22 shows the Well A interpolated velocity with the maximum allowed perturbation and the search region between two time-depth curves derived from the bound velocities. We create the lower bound curve using lower velocity, $V_{slow} = V_P * 0.8$, and the upper bound curve derives from the higher velocity, $V_{upper} = V_P * 1.2$. The attenuation is time dependent then, by using this approach, most of the seismogram attenuated region stays outside of the search region (e.g., Figure 22-b), maintaining only amplitudes and frequencies near where the wavelet frequency has been estimated - in the case of the Well A the last prominent peak.

Figure 22 – a) Interpolated velocity log with the maximum allowed perturbation region (gray region). b) The search region inside both time-depth curves (top) and the part of the seismic trace that comprehends the search region (bottom). Data from Well A.

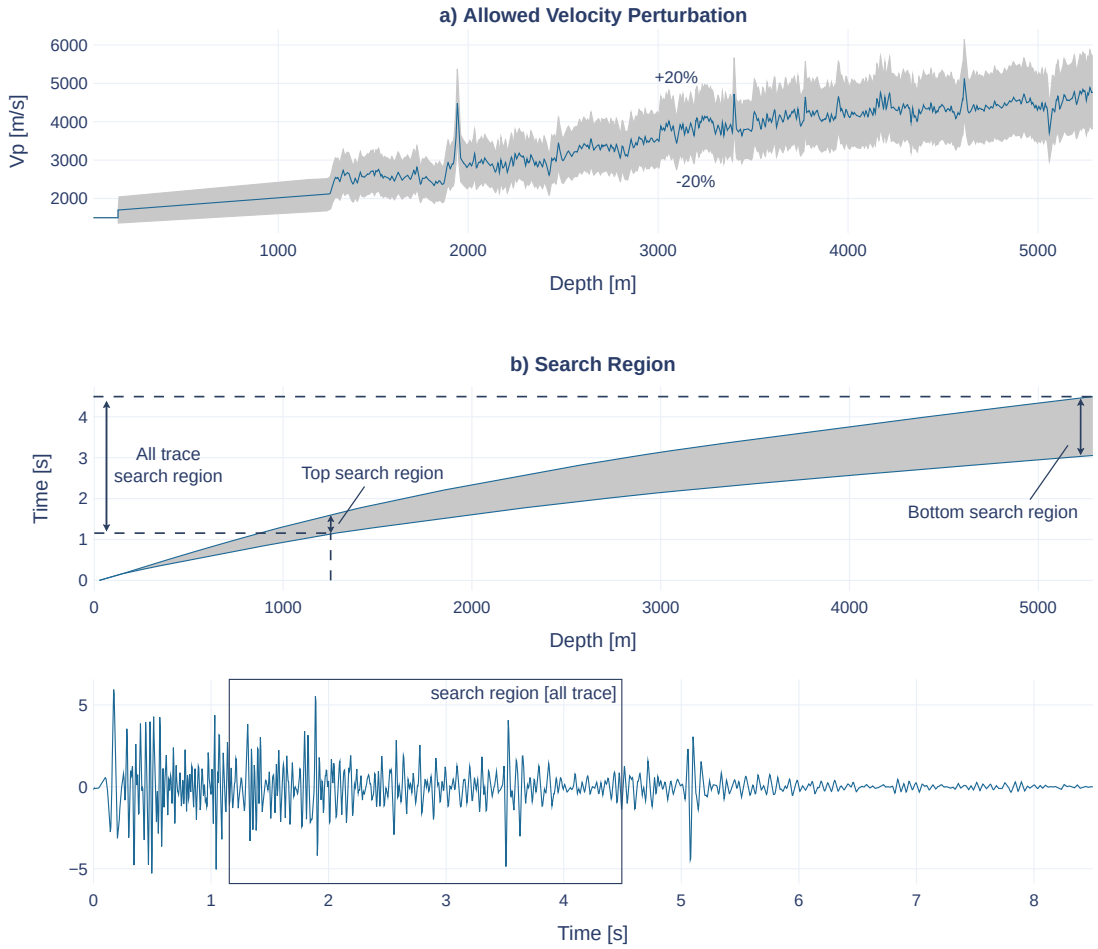

Source: Author

This work proposes three estimation methods based on the search region, one for each

identified misalignment scenario. The sequence of operation to estimate the matching region is presented in the Algorithm 1, where well data correspond to the velocity log, density log, and Ricker frequency at the interest region. The hyper-parameters are filter sizes, the wavelet size, and the time shift of the bulk shift. We detail their values in section 4.2.

Algorithm 1 Estimation of the matching region

Require: Hyper-parameters, well data, seismic trace, method

Pre-processing the well logs. *parameters*: hyper-parameters, well data.
Compute the seismic search region. *parameters*: lower and upper velocity log.
Compute the synthetic trace and remove the interpolated region.
if method = "all trace" **then** ▷ All trace method
    DTW(seismic trace, synthetic trace, search region).
else if method = "bottom DTW" **then** ▷ Bottom DTW method
    Crop the bottom region of the synthetic and seismic trace.
    DTW(seismic's bottom trace, synthetic's bottom trace)
    Extract the bottom's position
    DTW(seismic trace, synthetic trace, search region, bottom's position)
else ▷ TWDTW method
    Crop the bottom region of the synthetic and seismic trace.
    Compute the weighted distance matrix δ_ω.
    TWDTW(seismic's bottom trace, synthetic's bottom trace, δ_ω)
    Extract the bottom's position
    DTW(seismic trace, synthetic trace, search region, bottom's position)
end if
Compute the correlation of the final DTW alignment.
Extract the matching region from the final warping path.
return Matching region and the alignment's correlation

Before applying the DTW, we crop the synthetic and seismic traces in all scenarios. In the synthetic trace, we remove the velocity log interpolated region (e.g., the constant part shown in Figure 21), while in the seismic trace, is removed the part outside the search region. The first scenario refers to when the synthetic and seismic trace has a base reflector indicating the interest region with the same magnitude concerning the neighborhood. We apply the DTW algorithm with the begin and end opened to remove part of the seismic trace that is not present in the synthetic trace. For this step, the focus of the DTW is not the alignment itself but its position.

With the search region, most of the attenuated regions stay outside the search region. However, the amplitude of prominent reflectors compared to their neighborhood can differ, leading to misalignment. For these cases, we propose a bottom-first estimation method. This method first estimates the well's bottom position using DTW with the beginning and end opened to discard part of the seismic trace that does not exist in the synthetic trace. We search the bottom's position by aligning the last 15% of the synthetic trace with

the bottom search region of the seismic trace that is defined by the difference between the final time of the slower and faster time-depth curve, as shown in Figure 22-b. Then, with the bottom position fixed, the remaining data is removed. After, from the bottom position, all the trace synthetic trace (with the interpolation removed) is aligned using DTW with begin opened to estimate the top position and end closed.

The case where both traces do not have a prominent reflector near the well bottom region is the last identified case and the most difficult. For this scenario, our method relies on the hypothesis that the matching region tends to be near the first interpolated synthetic trace. This approach is similar to the second one but uses a TWDTW (MAUS et al., 2016). In the original version, TWDTW adds a temporal cost to the cost matrix based on a linear or logistic model. Here, the temporal cost subtracts a percentage of the cost matrix δ. The temporal cost is based on a normal cumulative distribution function (CDF), ϕ, as described below:

$$\begin{aligned} \Phi(i,j) &= [1 - \phi(|i-j|)] \\ \delta_\omega(s_i, q_j) &= \delta(s_i, q_j) - \delta(s_i, q_j)\Phi(i,j)\beta \end{aligned} \tag{30}$$

where Φ corresponds to the inverse of normal CDF (to vary the CDF from 1 to 0), and $|i-j|$, is the temporal distance between the sample s_i (seismic trace) and q_j (synthetic trace). β limits the maximum percentage of the temporal cost. The default value for β is 0.5, then if $|i-j| = 0$ the value of the matrix cell $\delta_\omega(s_i, q_j)$ is reduced in 50%.

As the temporal distance increases, the reduction percentage decreases, as shown in Figure 23 (left). Using the temporal cost, TWDTW prioritizes an alignment of the synthetic trace near its original position. However, far alignment is allowed if the distance exceeds the region under temporal cost influence. Different of a constrained DTW that constrains the alignment position inside a specific region. Figure 23 (right) shows the cumulative matrix cost difference between TWDTW and DTW, remembering a constrained window with smooth bounds.

4.2 Fine-tuning with Bayesian Optimization

Section 2.4 describes the steps needed to perform a well-to-seismic tie. During tying, geoscientists must adjust some parameters to increase the tie quality. To automate this process, we incorporated part of the Tschannen, Ghanim e Ettrich (2022) automation process, in which a Bayesian Optimization (BO) is used to find the optimum point in a parameter space. As described in section 3.4, BO is designed to efficiently tackle the trade-off between the exploration and exploitation process, becoming a standard algorithm for tuning hyperparameters in machine learning algorithms.

Following the original approach, we obtain the initial observation using a Sobol sequence - to provide a quasi-random sampling of the parameter space - and the Gaussian

Figure 23 – Temporal cost function regularized by $\beta = 0.5$ and centered in 0.1 (left), with the cumulative matrix cost difference between TWDTW and DTW for Well A (right).

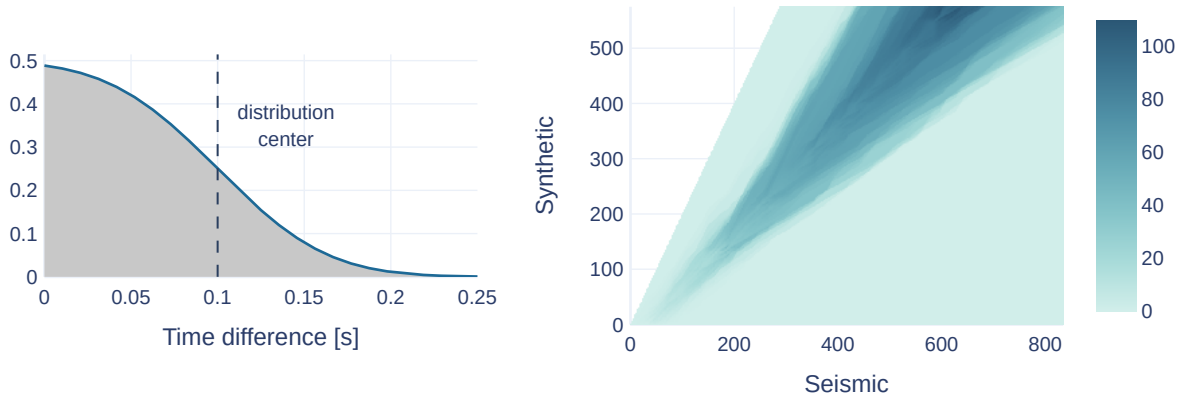

Source: Author

process (GP) (RASMUSSEN; WILLIAMS, 2006) is used as the surrogate model to estimate the performance and uncertainties over the entire parameter space. We defined a simple 4-dimensional parameter space to be optimized. The first two parameters are the despiking and smoothing window length, constrained between 31 and 61 samples. The third parameter is the source wavelet length used to construct the synthetic seismic trace, constrained between 204 ms and 324 ms. The final parameter is the time-depth bulk shift constrained between ±200 ms.

We have chosen the parameter bounds such that the minimum values result in a reduced, or almost no effect, on the data. At the same time, the maximum represents a probable limit that a meaningful signal may be lost. All prior distributions are uniform over the specified ranges. At each iteration, the BO computes the correlation coefficient of the estimated matching region. Based on this value, the posterior likelihood is updated to favor the relevant regions regarding performance and uncertainty. We also set the number of iterations to 80 with a ratio of 60% of random search as 40% of Bayesian updates.

4.3 Segmented matching strategy with global optimization

After estimating the matching region by one of the three proposed methods, using fine-tuning or not, the next step consists of matching the synthetic with the seismic data. This section presents our segmented matching strategy, which uses global optimization to estimate a perturbation curve to modify the velocity log and constructs a synthetic trace more similar to the seismic trace. This matching strategy is based on the Gelpi,

Pérez e Velis (2020) work, while the well and seismic trace segmentation is based on the alignment path of the constrained DTW (HERRERA; BAAN, 2014).

4.3.1 Non-segmented matching approach

The tie results performed with the Gelpi, Pérez e Velis (2020) original method will be presented, justifying our proposed modifications. After this point, the original approach will be called DE-tie to facilitate its identification. In the experiments performed on DE-tie original works, the tie procedure was performed on an onshore well with a depth length varying from approximately 700 to 1500 meters. These characteristics differ significantly from our set of six wells: A, B, C, E, F, and G - offshore wells with depths of approximately two to three times greater.

Once initially it is not possible to know the optimal parameter for each well, we chose to evaluate different combinations of knots number, $M = [3, 5, 7, 10, 15]$, and maximal velocity distortion, $P = [5\%, 10\%, 15\%, 20\%]$. These vectors were defined empirically based on the trade-off between search space size and execution time. Regarding phase rotation, two scenarios were analyzed: with and without rotation. In tests with rotation, a range of $[-90°, 90°]$ was set as the maximum allowable rotation. All tests used two stopping criteria: the cost function convergence and a maximum number of generations equal to $1,000$.

In Figura 24, the obtained correlation for each tested well is shown. Anyone of the wells achieved an acceptable correlation coefficient[2], above 0.7. At the same time, most correlations are concentrated between 0.2 and 0.6, indicating that the method cannot obtain good correlations in this set of wells. The mean correlation with rotation is 0.440, and 0.417 for experiments without phase rotation. In most cases, not performing phase rotation does not impact the final result. Only in Well E does the phase rotation impact the correlation.

When we analyze the influence of each parameter on the correlation obtained, as described in the original work, it is observed that a higher number of knots leads to a higher correlation once more knots increase the capability of the method to perturb the velocity profile. Our experiments show a positive trend for the relation between knots and obtained correlation. Then, the method can obtain an acceptable correlation coefficient if the optimization uses enough knots, as shown in Figure 25.

Once this method relies on a global optimization algorithm, increasing the search space's dimension can lead to an undesired execution time. To verify this behavior, we plotted the execution time for each configuration, Figure 26. As expected, we observe an exponential growth in the processing time needed to align both signals in comparison with the short linear correlation increment. Therefore, the required execution time of

[2] This value was defined by a Petrobras geologist, a partner in this study

Figure 24 – Obtained correlation in each well ordered by depth length. The dashed horizontal line indicates the acceptable level of correlation obtained after a well-to-seismic tie.

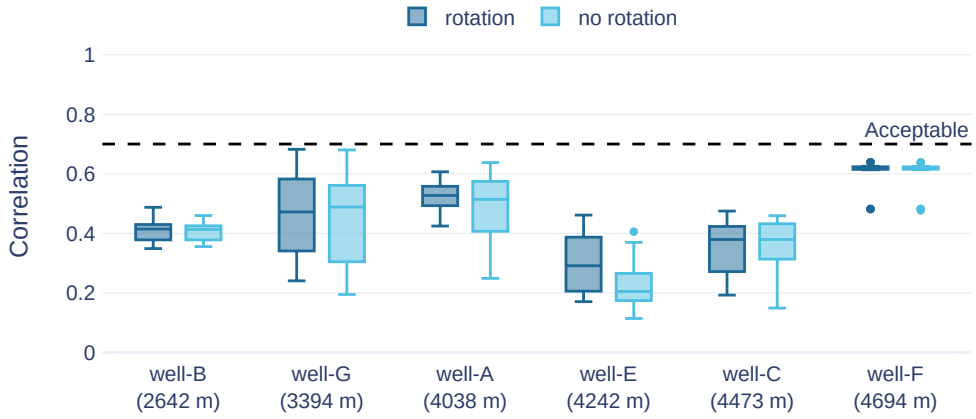

Source: Author

Figure 25 – Obtained correlation for all wells varying the number of knots, M.

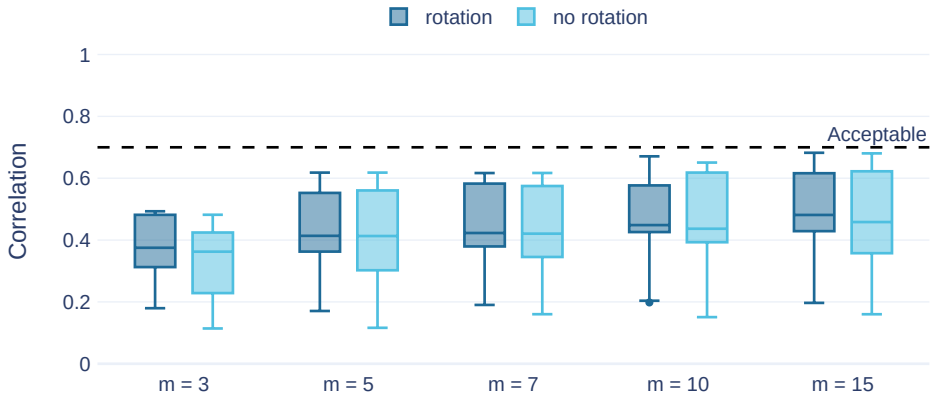

Source: Author

simply growing the number of knots does not compensate for the correlation coefficient increment.

4.3.2 Segmentation of the well with Constrained DTW

Since significantly increasing the number of knots used to construct the $p(z)$ function is not feasible, reducing the depth interval where the optimization is applied through segmentation is proposed. This segmentation allows us to increase the entire well ratio of knots number per corrected depth interval. For example, if we segment the well into six parts, the knots used to construct the perturbation curve are increased sixfold with a linear increment in the execution time. A higher number of knots allows a finer adjustment

Figure 26 – The execution time to process all six wells for each parameter configuration tested. Executions without phase rotation presented a reduced execution time.

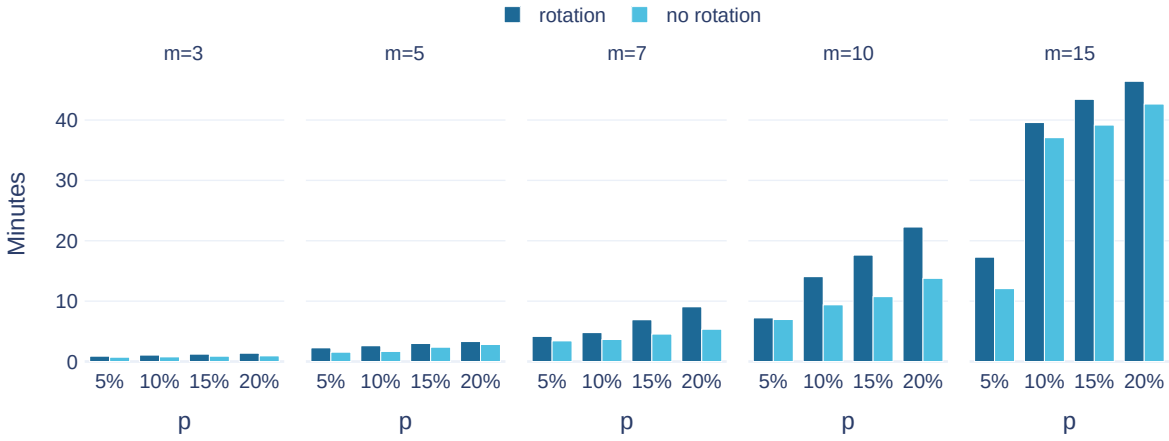

Source: Author

in the velocity log. The number of segments is an arbitrary parameter defined by the user. Most wells, except well G, were segmented into six parts. The number of segments was determined based on the number of samples in both seismic and synthetic trace present in each segment, ensuring that it is not smaller than the wavelet used in the convolution.

The seismogram is divided into K equal-sized parts in the segmentation process. The tying process assumes that both seismograms represent the same set of physical phenomena (NEWRICK, 2012). Then, each segment of the seismic trace has a corresponding region in the synthetic one, which is associated with the well's depth. The seismic-synthetic correspondence is one product of the tying process, the time-depth relationship. An initial time-depth estimation can be achieved using the constrained DTW algorithm for segmentation proposes. Once the estimated time-depth curve is not used to reconstruct or perturb the velocity logs, the warping produced during the matching can be relaxed. The velocity correction is made only by the perturbation curve.

After performing the constrained DTW, the warping path is used to construct the initial time-depth curve. We can segment the well into K parts with the correspondence between both traces. The bounds of each segment are defined by positioning $K-1$ equidistant points over the seismic trace, for each of these segmentation points is associated, through the time-depth curve, with a well's depth. Now, we have the same segmentation points in both domains, well and seismic data. Thus, each segment of the seismogram has a corresponding well segment. Figure 27 illustrates the segmentation process.

Figure 27 – Constrained DTW segments of the Well A. The time-depth curve starts at 1.33 seconds because of the interpolated region removal.

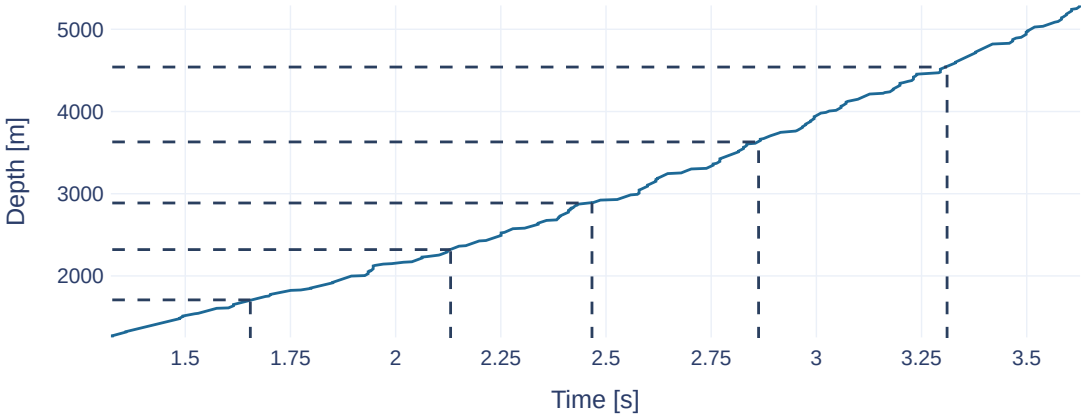

Source: Author

4.3.3 Segmented matching approach

We have the well segmented in the depth and time domain at this stage. Therefore, we can construct a perturbation curve $p(z)$ capable of correcting a specific segment. Through the relationship established with the constrained DTW, we already know in advance which region of the seismogram will be corrected by each segment correction. We can place m fixed knots at constant depth intervals along the selected segment and apply a global optimization algorithm to estimate the best $p(z)$ curve. As we correct the segments, they are concatenated with the already corrected ones.

During the experiments, we defined two objective optimization function, the same used initially by DE-tie and a proposed variation that include a trace size factor. The original cost function proposed by Gelpi, Pérez e Velis (2020) is the inverse of the Pearson correlation coefficient, that is, $J(S, Q) = 1 - \gamma$, where γ is the correlation between both traces S and Q. However, during the optimization process, the entire velocity of the well can be increased, affecting the synthetic trace duration. Once the velocity log is inversely proportional to the trace duration time, an increment can result in a synthetic trace shorter than the seismic and consequently losing the interest region - usually localized at the bottom of the seismic trace. To mitigate this effect, we proposed the cost function described below:

$$J_\omega(S, Q) = (1 - \gamma) + \phi(\text{t\_diff}(S, Q)) \tag{31}$$

where ϕ is a normal CDF, and t_diff is time duration difference between both traces. Like our third matching region estimation method, ϕ penalizes the correlation as t_diff increases. If t_diff $= 0$, we have the original DE-tie cost function. Both cost functions

depend on the correlation coefficient, requiring both series to have the same size. In J, if the signals have different sizes, the correlation is computed based on the short signal size. In contrast, for J_ω, the correlation is calculated only within the corresponding segment region already corrected. This process is carried out iteratively and sequentially from the top segment to the base of the well.

Figure 28 presents the proposed segmented matching strategy for the well A status when its velocity is corrected until segment 3. As mentioned, the segments are corrected sequentially, meaning that when the global optimizer starts correcting the velocity segment 3 (blue region in the velocity curve), 1 and 2 are already corrected - no further modifications are made. We update the knot's amplitude during each iteration of the segment's optimizing process and construct the synthetic trace using the entire velocity log (even the non-corrected region). However, for the segment cost function, the correlation is computed using only the region from the well's top to the lower bound of the segment, which corresponds to the region already corrected. For example, in Figure 28, this region corresponds to the blue region in the seismic trace.

Figure 28 – Correction of the Well A velocity log through the segmented matching approach. The blue region in the seismic trace (top) represents the region used to compute the correlation coefficient. The current corrected segment is the blue region in the velocity log (bottom).

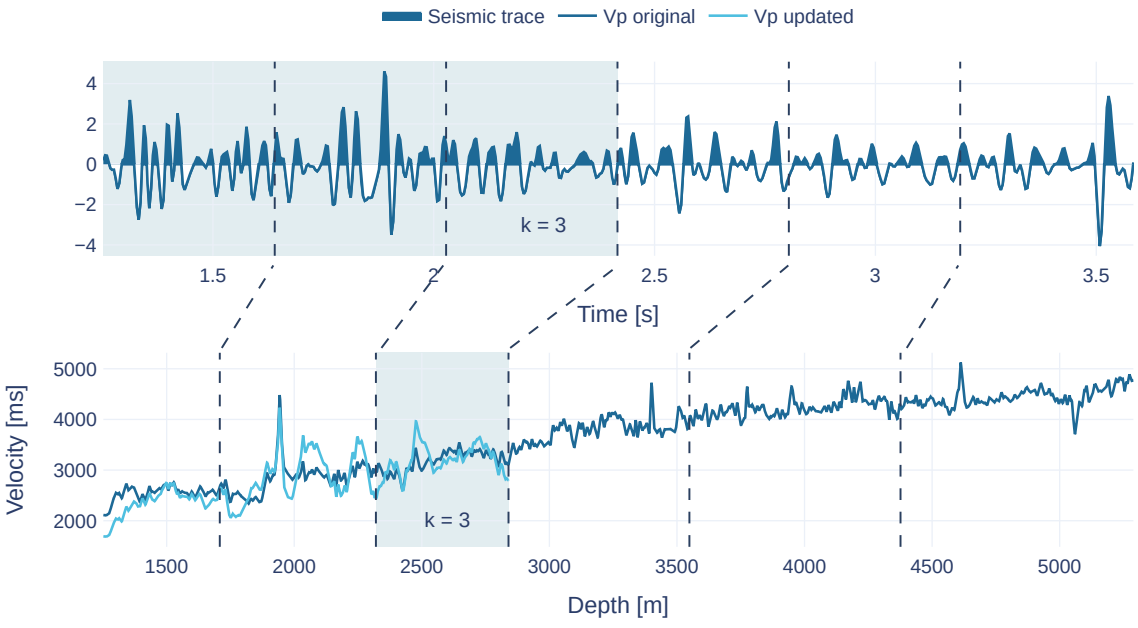

Source: Author

Performing a sequential velocity correction allows us to utilize the information from previously corrected segments, preventing the occurrence of discontinuities in the $p(z)$ curve at the boundary between segments. Except for the first segment, the current segment's first node corresponds to the previous one's last knot and remains unchanged

during optimization. Every segment bound contains a shared knot. Figure 29 shows the $p(z)$ curve constructed until segment 3 for well A.

Figure 29 – Example of segmented velocity correction until segment 3 (left) and its respective $p(z)$ curve (right).

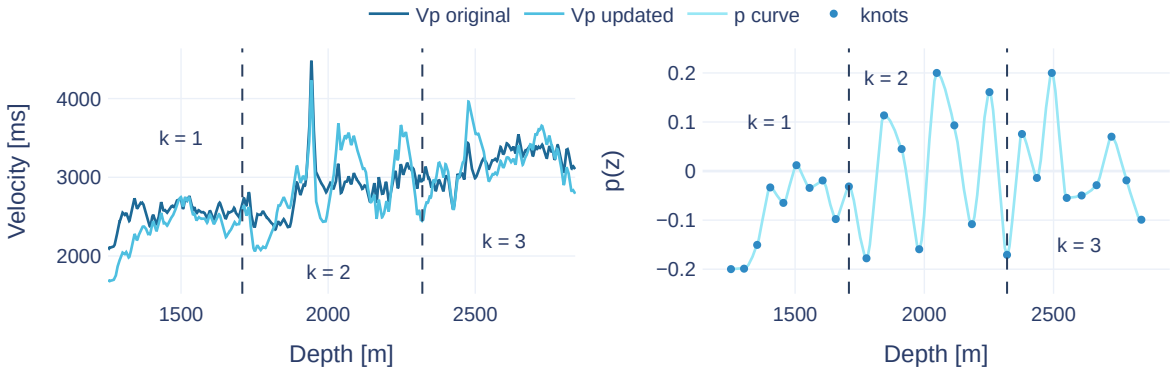

Source: Author

4.4 Experimental evaluation

As described in the subsection 4.3.1, a set of six offshore wells was obtained through a partnership with Petrobras company for the experiments in the work. Each well contains the sonic and density logs and the Ricker frequency at the interest region. All pre-processing procedures applied in the wells are described in the section 2.4 (e.g., the filtering, the estimation of missing values, and the removal of spurious values). When the Bayesian fine-tuning was not applied, the despike and smoothing filter size was 51 samples, with no bulk-shift application, and using a Ricker wavelet of 300 ms. All these values are the default for the six wells and have been estimated with Petrobras's geologists through a manual tying procedure and using information on neighborhood wells (e.g., its check-shot series or extrapolating its well top and bottom).

4.4.1 Matching region estimation

This work compares our three proposed methods to find the matching region with the manual estimation. The matching region's top and bottom positions were estimated using or not fine-tuning. Table 1 presents all the experiment results. Well A is the easiest to estimate the top and bottom due to the shape of both traces being very similar in frequency and amplitude. All methods variation was able to estimate its matching region with an error lower than 25 ms. In Well F, the bottom reflector is very expressive, allowing all methods to estimate the bottom position of the matching region. However, the Well

F top region has a considerable amplitude difference compared to the seismic trace. All methods estimated the top position ≈ 150 ms further the manual estimation.

Table 1 – Results obtained by the matching region estimation with the proposed methods. All values presented are in seconds. Bold values represent a correct estimation of the matching region's top or bottom position. *The estimated position is better than the manually defined one. +The estimated position is near the correct one.

Well	**Manual**		**All trace**		**Bottom DTW**		**TWDTW**	
	Top	Bottom	Top	Bottom	Top	Bottom	Top	Bottom
A	1.254	3.59	**1.276**	**3.616**	**1.276**	**3.612**	**1.276**	**3.612**
B	1.492	3.14	1.9	3.368	1.8	3.364	1.8	3.364
C	0.472	3.404	0.768	**3.388**	0.772	3.692	0.772	3.692
E	0.472	3.397	1.056	3.812	**0.524**$^{+}$	3.484	**0.524**$^{+}$	3.484
F	0.488	3.573	0.632	**3.568**	0.632	**3.564**	0.632	**3.564**
G	1.922	3.605	1.728	**3.68***	1.408	**3.676***	1.408	**3.676***
Well	**Manual**		**Bayesian Optimization**					
A	1.254	3.59	**1.268**	**3.616**	**1.276**	**3.612**	**1.272**	**3.612**
B	1.492	3.14	1.892	3.368	1.828	3.364	1.836	3.364
C	0.472	3.404	0.768	**3.384**	0.58	3.692	0.58	**3.388**
E	0.472	3.397	**0.524**$^{+}$	3.496	**0.524**$^{+}$	3.488	**0.524**$^{+}$	3.488
F	0.488	3.573	0.632	**3.568**	0.64	**3.564**	0.632	**3.564**
G	1.922	3.605	1.64	**3.68***	1.64	**3.672***	1.64	**3.672***

Source: Author

While fine-tuning does not increase the method performance for Well A and Well F, its influence is perceptive in Well C. After the fine-tuning process, the TWDTW method can find the correct bottom position with an error of ≈ 16 ms and the estimated top position is closer than without the optimization. In both cases, using or not fine-tuning, the method "all trace" can also estimate the bottom position, but its top position is less accurate. In Well G, all methods can identify the correct bottom position. The difference presented in Table 1 is due to the excess of data present in the synthetic trace, Figure 30. During the manual estimation, the bottom selected is close to the interest region (the last peak), but the well is more profound than the interest reflector. All methods missed the top region of this well, with the estimated top positioned earlier than the manual definition, increasing the duration of the synthetic trace.

In Well E, except for the method "all trace", the estimated top and bottom positions were near to the manually defined. The top was estimated ≈ 52 ms ahead of the correct one, which can be considered close enough due to the difficulties present in the top of the well, e.g., interpolated region, differences in the frequency and amplitude when compared with the region where the wavelet is estimated. The estimation error is higher for the bottom, ≈ 100 ms further than the correct position, causing a peak misalignment. The Well E bottom error is probably because of the shape differences between the synthetic's

Figure 30 – The estimated matching region of the Well G with the method "all trace". We can see the excess of data at the end of the synthetic trace.

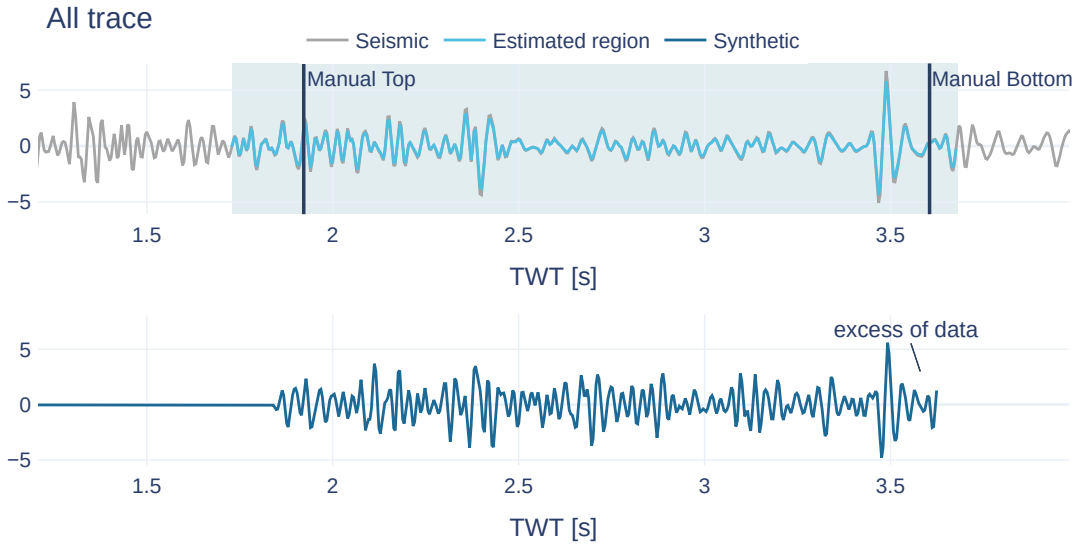

Source: Author

last part and the seismic trace's interest region.

Figure 31 – The estimated matching region of the Well E with the method Bottom DTW. At the end of the synthetic trace, we can see both traces' shape and amplitude differences.

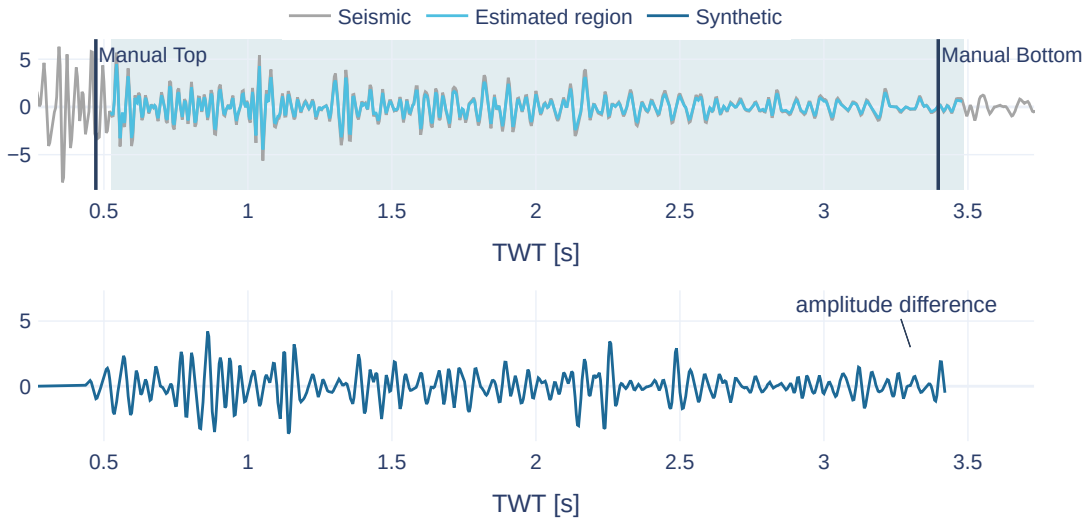

Source: Author

None of the proposed methods could identify the Well B matching region position. Together with Well G, Well B has a lot of missing values at the well top region, with both starting respectively at ≈ 1900 and ≈ 2000 meters. The excess missing values reduce the capacity to estimate the top region once we define the search region through interpolation, making the correct top stay outside the top search region. Also, both wells do not have

a prominent reflection peak indicating the interest region in the seismic trace, making it hard to DTW align with the correspondent reflector peak of the synthetic trace. In Well B, the constructed synthetic and the seismic trace have a considerable shape difference.

4.4.2 Segmented matching approach

Our segmented matching approach was also executed in the six wells previously described. In these experiments, we used the manually defined matching region once the matching approach using global optimization could not shift the well's top position during the optimization process. From now on, the proposed segmented matching approach will be called SegTie-DE to facilitate the identification. To verify their influence on the alignment approach with optimization, we tested two different parameter definition strategies, one with phase rotation and the other without phase rotation. In both cases, all segments have the same parameters for the segmented version. We also tested using other global optimization algorithms and a grid search to estimate the best parameter configuration for each well's segment. The parameters search space used is the same as the DE-tie experiments: knots number $M = [3, 5, 7, 10, 15]$, maximal velocity distortion $P = [5\%, 10\%, 15\%, 20\%]$, and maximum phase rotation angle $R = [-90°, 90°]$.

The first experiment compares our proposed segmented approach with the non-segmented one. Figure 32 shows the best correlation obtained for each well using all the fourth tying methods, two segmented (SegTie-DE) and two non-segmented (DE-tie). The use of segmentation improved the final correlation coefficient in all cases. Figure 32-a presents the execution of the optimization using the original cost function, the inverse of the Pearson correlation, which has obtained the best correlations in all wells. Figure 32-b, on the other hand, shows the best correlation with the use of our proposed cost function, Pearson correlation weighted by the size difference between the final synthetic and seismic trace (Equation 31). As suspected, a reduction in the final correlation occurs once the optimization also needs to focus on the synthetic trace size, limiting how much the velocity log can be perturbed.

With Well B, we analyzed the impact of the proposed cost function in the alignment process, aside from the correlation. Well B has the shortest synthetic trace in our set of wells with its seismic trace, Figure 33-a. The impact of the proposed cost is evident in the DE-tie. With its use, the final synthetic trace has almost the same size as the seismic trace and matches the interest region (Figure 33-b). However, the perturbation could not match the trace peaks, causing a reduction in the final correlation. The size of the trace impacted the optimization more than the correlation value. In the SegTie-DE, the correlation was prioritized, neglecting the synthetic size (Figure 33-c), probably due to how we compute the correlation during the sequential matching. As described before, we compute the cost function considering only the already optimized region during the

Figure 32 – Performance of the DE-tie and SegTie-DE. a) Presents the correlation obtained using the original Pearson correlation as a cost function, while (b) uses weighted Pearson correlation.

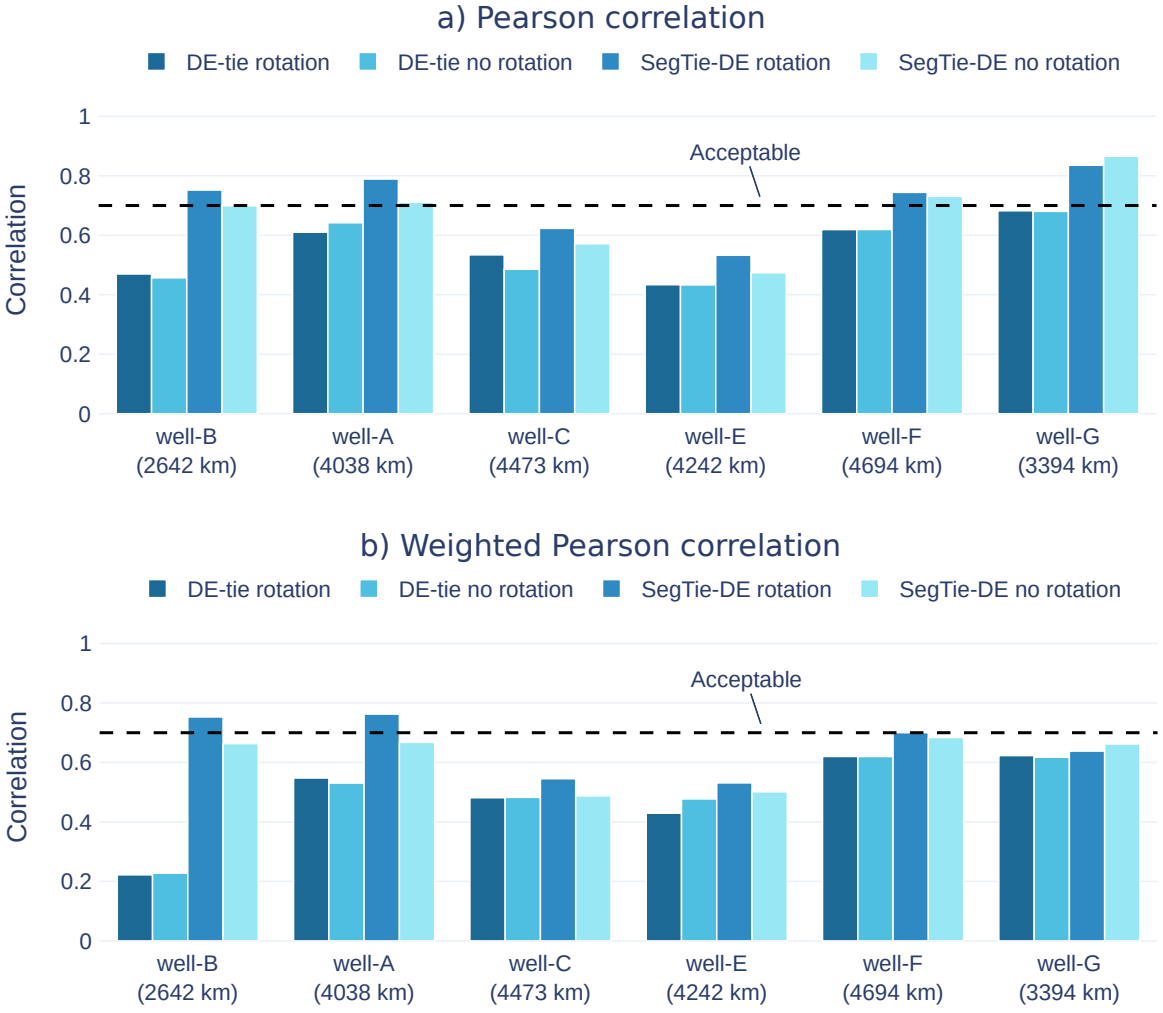

Source: Author

optimization process. This way, when the optimizer is on the last segment, it cannot increase the overall velocity to squeeze the synthetic trace size.

The proposed cost function does not impact the method execution time. Table 2 presents the execution time, in minutes, of the fourth variation of the non-segmented and segmented approach. The non-segmented approach is identified by DE-tie and the segmented one by SegTie-DE. The "I" indicates Pearson correlation as a cost function, and "II" is the proposed weighted Pearson correlation. The *phase* indicates the use of phase rotation. Most of the impact in the execution time falls on the segmentation process, which increases the number of optimizer executions. Among the wells experimented, Well G is an outlier when concerned about execution time. In all methods, our convergence is not good enough, requiring a considerable amount of time to execute trace alignment,

Figure 33 – Impact of the proposed cost function in the Well B. a) Initial synthetic trace position, estimated by the top well velocity interpolation. Best execution of the DE-tie (b) and SegTie-DE (c) with the proposed cost function. In both cases is used phase rotation.

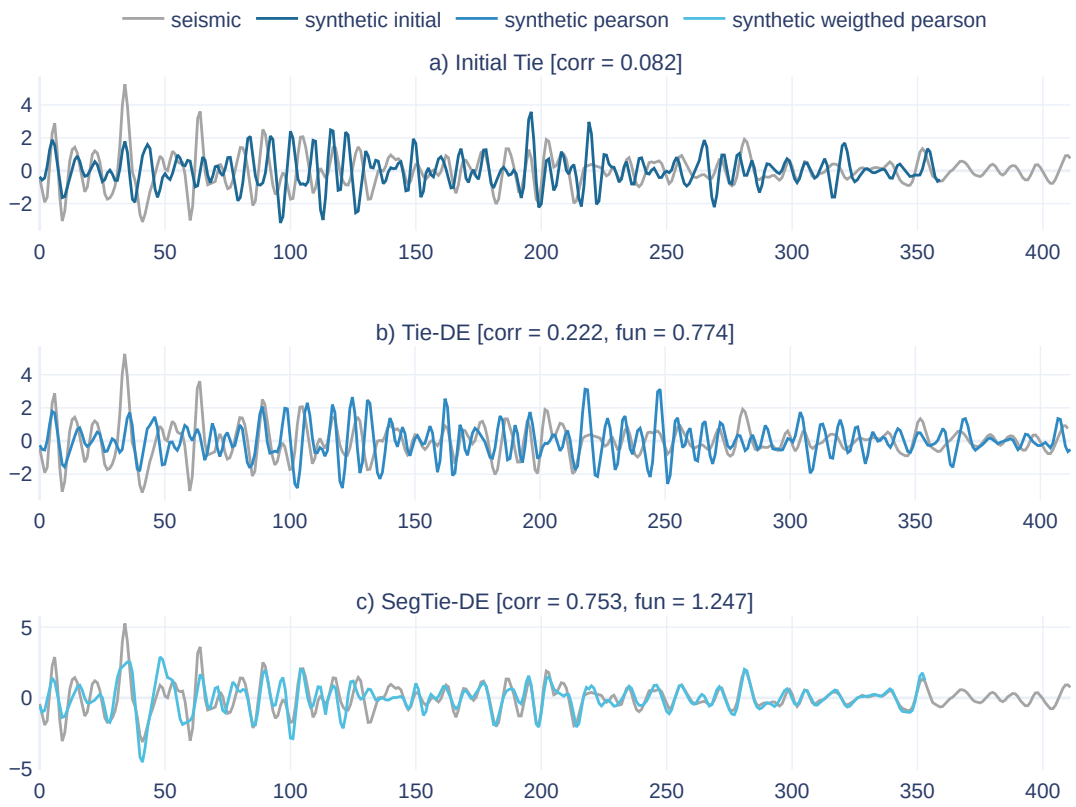

Source: Author

finishing its execution due to achieving the maximum generation (1000 generations). The segmentation increased the general execution time from $\approx$ 5 minutes to approximately $25 \sim 30$ minutes per well.

The proposed tying process has the advantage that the execution steps are highly independent, allowing the use of a different optimizer if necessary. Our proposed alignment method, as DE-tie, is independent of the optimization algorithm used to estimate the $p(z)$. Considering this scenario, we made an exploratory experiment to verify using Particle Swarm Optimization (PSO) as an optimizer. PSO is a stochastic optimization technique based on swarm that simulates the behavior of social animals, and like DE, it is also an evolutionary algorithm (WANG; TAN; LIU, 2018). The results are not promising, as shown in Figure 34. With the PSO optimizer, the method could not achieve an acceptable correlation level in all wells. The lack of performance is even higher when using the weighted Pearson correlation. Considering the reduced execution time and achieved correlation, compared with DE, the PSO has been stopped early due to non-convergence of the cost function. In all scenarios, the SegTie-PSO had a higher correlation than the

Table 2 – Comparison of the execution time between the non-segmented and segmented alignment approach. The values are in minutes and represent the model's best execution, with the higher correlation, in the respective well. The *phase* indicates the use of phase rotation.

Model	Well A	Well B	Well C	Well E	Well F	Well G
DE-tie I *phase*	3.96	1.34	4.69	1.81	3.22	31.39
DE-tie I	3.73	1.58	4.18	0.72	3.18	28.57
DE-tie II *phase*	5.48	0.44	5.34	4.32	5.04	13.05
DE-tie II	1.61	0.36	5.74	5.37	4.01	11.53
SegTie-DE I *phase*	29.13	13.56	25.35	24.01	30.81	185.27
SegTie-DE I	21.06	13.22	18.54	16.60	26.67	198.19
SegTie-DE II *phase*	40.90	10.96	34.75	31.30	33.29	97.21
SegTie-DE II	28.04	9.46	22.16	22.34	27.57	88.20

Source: Author

PSO-tie.

Our experiments also tested the use of different configurations for each segment. For each segment, were tested all parameter combinations through a grid search. Figure 35 shows the obtained correlation with SegTie-DE and SegTie-PSO. The "grid" at the legend indicates using grid search to estimate the best parameters for each segment. Using grid search does not increase the final well's correlation compared with a conventional approach (Figure 35-a). Only the version with PSO showed differences. In most cases, the combination PSO and grid search reduced the correlation achieved in the well. The similarity between the correlations obtained with DE is explained by Figure 35-b. Except for Well E and B, the grid search selected the same number of knots that the conventional SegTie-DE, indicating that, in general, the best configuration consists of selecting the highest number of knots possible.

4.5 Final considerations

This chapter presented our partial automation of the well-seismic tying process by estimating the matching region and our main contributions. The first contribution consists of creating three methods to estimate the matching region of the well with the seismic data based on DTW. Besides the limitations of the matching region estimation based exclusively on the shape of the traces, our methods can make good approximations in most of the wells. In Well A, all methods were able to precisely estimate the matching region's top and bottom and even correct the manual bottom position estimated at Well G. The limitation of the matching region estimation algorithm is our exclusive look at the trace's shape, being unable to correctly estimate the region in wells the synthetic trace and seismic trace are different, or that does not have a prominent reflection at bottom.

A secondary contribution is the incorporation of the Tschannen, Ghanim e Ettrich

Figure 34 – Performance of the PSO-tie and SegTie-PSO. a) Presents the correlation obtained using the Pearson correlation as a cost function, while (b) uses weighted Pearson correlation.

Source: Author

(2022) fine-tuning flow to estimate the tying hyper-parameter when they are unknown or want to increase the correlation of the initial synthetic trace with the seismic trace. Using fine-tuning increased the methods' precision in estimating the matching region's top position. Another main contribution is the algorithm to segment the well and the seismic data. In that way, each well's segment has a corresponding seismic segment. The segmentation algorithm is inspired by the Constrained DTW algorithm for well-seismic tying proposed by Herrera e Baan (2014).

Incorporating the segmentation in the well-seismic tying method proposed by Gelpi, Pérez e Velis (2020) increased the correlation coefficient obtained in an offshore well. Besides not being widely explored in this work due to our scope, a side effect of the segmentation is using different wavelets along the well, one for each segment, simulating

Figure 35 – Impact of the grid search in the obtained correlation (a) and the number of knots used to construct the $p(z)$ function (b).

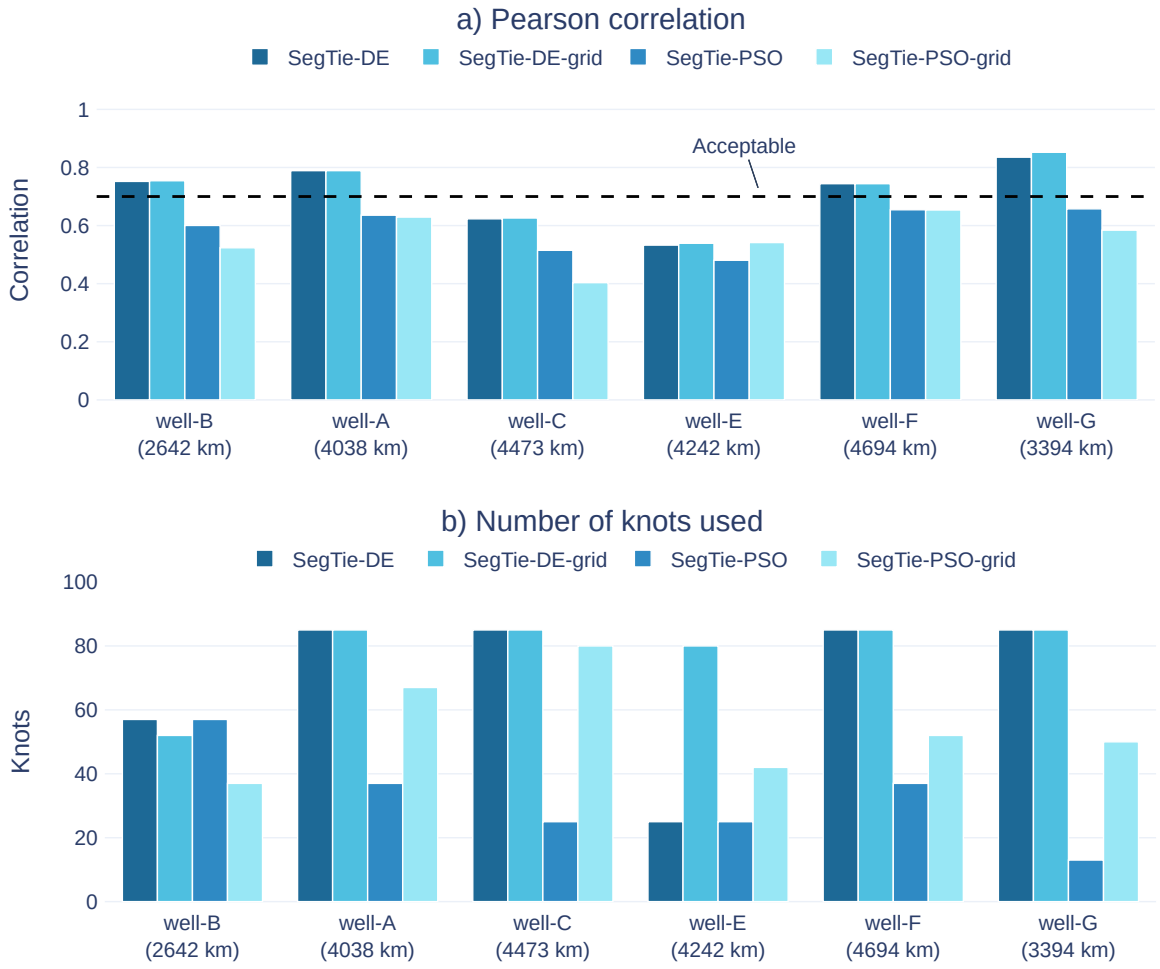

Source: Author

a non-stationary wavelet. During the construction of the segmented alignment approach, we also proposed a second cost function, weighted Pearson correlation, that considers the final size of the synthetic.

Conclusion

In petroleum and gas exploration, interpretation activities develop a fundamental role. The seismic amplitude interpretation is an essential component of technical evaluation in exploring hydrocarbons. This interpretation process involves the integration of different sources of data. The well-to-seismic tie process is an essential interpretation tool that aims to associate the well data, recorded at the depth domain, with the seismic data in the time domain. The main contribution of this work is the partial automation of the well-seismic tying process with the estimation of the matching region. Automation reduces the necessary work spent in the well-seismic tie and removes the subjective aspects of the process. Section 2.4 presents the complete workflow used in this work. As discussed, the principal well-seismic tie methods still have limitations in constructing a fully automatic workflow.

Most of these limitations lead to unrealistic distortions at the velocity log, requiring geologic markers that are not always available or do not achieve satisfactory correlation in offshore wells with depth size. Also, most works consider that the user already knows the seismic matching region, which is only sometimes valid. The chosen alignment method, based on optimization, was made due to its higher capacity to maintain the velocity under control in the absence of geological markers or human intervention during the alignment. In its original form, the method presented a low performance in offshore wells with a depth higher than the one used in the original work. The method performance depends on the number of knots used to interpolate the perturbation curve, a parameter limited by the execution time. Most of these problems are mitigated by segmenting the well and seismic data using the Constrained DTW.

However, in both cases, segmented or not, the method cannot apply shifts at the initial top position, influencing its capacity to achieve a correct alignment and requiring an excellent matching region estimation. The proposed estimation method correctly identified the bottom position of the matching region in 5 wells of 6 and corrected the manual estimation of Well G's bottom position. Despite the difficulty in estimating the top po-

sition of the wells, the use of BO to fine-tune the core tying process's hyper-parameters increased the precision of the estimations. The segmented tying approach surpassed the non-segmented one in all wells and achieved an acceptable correlation, higher than 70%, in 4 wells. The constraints in the optimization process maintain the modifications at the velocity log under the margin of 20%, the quality control, and the shared knots at the segment's bound guarantee the continuity of the curve $p(z)$. Even though the weighted Pearson correlation cost function does not increase the overall correlation of the tying process, it has demonstrated the potential to increase the tie's quality.

During the development of the dissertation a publication of the experiment's initial results, as enumerated below:

1. "Uma análise da amarração poço-sísmica automática utilizando *Differential Evolution*", published at the IX Simpósio Brasileiro de Geofísica (SimBGf) in 2022, without Qualis CAPES (Coordenação de Aperfeiçoamento de Pessoal de Nível Superior) for Computer Science until the conclusion of the present text.

In future works, we can cite the improvement of the proposed methods to estimate the matching region. The exclusive use of the shape during the estimation limits its application if wells do not have traces with similar shapes or prominent peaks at the interest region. Reducing the bottom search region using additional information can lead to better estimations. About the segmented alignment with optimization, the incorporation of estimation wavelets models in our automation process to use the alignment method's capability to receive different wavelets for each segment. Multiple wavelets, each estimated at a different level of the well, can mitigate the attenuation effect. Also, considering the computational cost of the segmented alignment, supplying the optimizer with an initial solution can reduce its execution time.

References

ADAMS, N. H. et al. Time series alignment for music information retrieval. In: **ISMIR**. [S.l.: s.n.], 2004.

CUI, T.; MARGRAVE, G. F. Seismic wavelet estimation. **CREWES Res Rep**, v. 26, p. 1–16, 2014.

DAU, H. A. et al. The ucr time series archive. **IEEE/CAA Journal of Automatica Sinica**, v. 6, n. 6, p. 1293–1305, 2019.

FOLGADO, D. et al. Tssearch: Time series subsequence search library. **SoftwareX**, v. 18, p. 101049, 2022. ISSN 2352-7110. Disponível em: <https://www.sciencedirect.com/science/article/pii/S2352711022000425>.

_____. Time alignment measurement for time series. **Pattern Recognition**, Elsevier, v. 81, p. 268–279, 2018.

GADALLAH, M. R.; FISHER, R. **Exploration geophysics**. [S.l.]: Springer Science & Business Media, 2008.

GARDNER, G.; GARDNER, L.; GREGORY, A. Formation velocity and density—the diagnostic basics for stratigraphic traps. **Geophysics**, Society of Exploration Geophysicists, v. 39, n. 6, p. 770–780, 1974.

GELPI, G. R.; PÉREZ, D. O.; VELIS, D. R. Automatic well tying and wavelet phase estimation with no waveform stretching or squeezing. **Geophysics**, Society of Exploration Geophysicists, v. 85, n. 3, p. D83–D91, 2020.

GHOLAMY, A.; KREINOVICH, V. Why ricker wavelets are successful in processing seismic data: Towards a theoretical explanation. In: IEEE. **2014 IEEE Symposium on Computational Intelligence for Engineering Solutions (CIES)**. [S.l.], 2014. p. 11–16.

HARTKE, B. Global optimization. **Wiley Interdisciplinary Reviews: Computational Molecular Science**, Wiley Online Library, v. 1, n. 6, p. 879–887, 2011.

HERRERA, R. H.; BAAN, M. van der. A semiautomatic method to tie well logs to seismic data. **Geophysics**, Society of Exploration Geophysicists, v. 79, n. 3, p. V47–V54, 2014.

LINER, C. L. **Elements of 3D seismology**. [S.l.]: Society of Exploration Geophysicists, 2016.

LINES, L. R.; NEWRICK, R. T. **Fundamentals of geophysical interpretation**. [S.l.]: Society of Exploration Geophysicists, 2004.

MARGRAVE, G. F. Why seismic-to-well ties are difficult. **the 25th Annual Report of the CREWES Project**, 2013.

MARSH, H.; RODRíGUEZ-REINOSO, F. Chapter 2 - activated carbon (origins). In: MARSH, H.; RODRíGUEZ-REINOSO, F. (Ed.). **Activated Carbon**. Oxford: Elsevier Science Ltd, 2006. p. 13–86. ISBN 978-0-08-044463-5. Disponível em: <https://www.sciencedirect.com/science/article/pii/B9780080444635500169>.

MAUS, V. et al. A time-weighted dynamic time warping method for land-use and land-cover mapping. **IEEE Journal of Selected Topics in Applied Earth Observations and Remote Sensing**, IEEE, v. 9, n. 8, p. 3729–3739, 2016.

MUNOZ, A.; HALE, D. Automatically tying well logs to seismic data. **CWP-725**, Citeseer, 2012.

NEWRICK, R. Well tie basics. **Well tie perfection**, v. 52, p. 104–107, 2012.

NWAFOR, B. O.; HERMANA, M. Harmonic extrapolation of seismic reflectivity spectrum for resolution enhancement: An insight from inas field, offshore malay basin. **Applied Sciences**, v. 12, n. 11, 2022. ISSN 2076-3417. Disponível em: <https://www.mdpi.com/2076-3417/12/11/5453>.

OLSZEWSKI, R. T. **Generalized feature extraction for structural pattern recognition in time-series data**. [S.l.]: Carnegie Mellon University, 2001.

RASMUSSEN, C. E.; WILLIAMS, C. K. I. **Gaussian processes for machine learning**. [S.l.]: MIT press Cambridge, MA, 2006.

SAKOE, H.; CHIBA, S. Dynamic programming algorithm optimization for spoken word recognition. **IEEE transactions on acoustics, speech, and signal processing**, IEEE, v. 26, n. 1, p. 43–49, 1978.

SILVA, D. F.; BATISTA, G. E. Speeding up all-pairwise dynamic time warping matrix calculation. In: SIAM. **Proceedings of the 2016 SIAM International Conference on Data Mining**. [S.l.], 2016. p. 837–845.

SILVA, D. F.; BATISTA, G. E.; KEOGH, E. Large-scale similarity-based time series mining. In: SBC. **Anais do XXXI Concurso de Teses e Dissertações**. [S.l.], 2018.

SIMM, R.; BACON, M. **Seismic amplitude: An interpreter's handbook**. [S.l.]: Cambridge University Press, 2014.

STORN, R.; PRICE, K. Differential evolution–a simple and efficient heuristic for global optimization over continuous spaces. **Journal of global optimization**, Springer, v. 11, n. 4, p. 341–359, 1997.

TÖRN, A.; ŽILINSKAS, A. Introduction. In: **Global Optimization**. Berlin, Heidelberg: Springer Berlin Heidelberg, 1989. p. 1–24. ISBN 978-3-540-46103-6. Disponível em: <https://doi.org/10.1007/3-540-50871-6_1>.

TSCHANNEN, V.; GHANIM, A.; ETTRICH, N. Partial automation of the seismic to well tie with deep learning and bayesian optimization. **Computers & Geosciences**, Elsevier, v. 164, p. 105120, 2022.

WANG, D.; TAN, D.; LIU, L. Particle swarm optimization algorithm: an overview. **Soft computing**, Springer, v. 22, p. 387–408, 2018.

WANG, K.; LOMASK, J.; SEGOVIA, F. Automatic, geologic layer-constrained well-seismic tie through blocked dynamic warping. **Interpretation**, Society of Exploration Geophysicists and American Association of Petroleum . . . , v. 5, n. 3, p. SJ81–SJ90, 2017.

WANG, Y. Frequencies of the ricker wavelet. **Geophysics**, Society of Exploration Geophysicists, v. 80, n. 2, p. A31–A37, 2015.

WHITE, R.; SIMM, R. Tutorial: Good practice in well ties. **First break**, European Association of Geoscientists & Engineers, v. 21, n. 10, 2003.

WU, H. et al. Improved seismic well tie by integrating variable-size window resampling with well-tie net. **Journal of Petroleum Science and Engineering**, Elsevier, v. 208, p. 109368, 2022.

YI, B. Y. et al. Comparison of wavelet estimation methods. **Geosciences Journal**, Springer, v. 17, n. 1, p. 55–63, 2013.